Authors: Manuel Toledano[1], Esther Muñoz-Soto[1], Fátima S. Aguilera[1], Estrella Osorio[1], Mayra C. Pérez-Álvarez[2], José AD. García-Menocal[2], Manuel Toledano-Osorio[1]*, Raquel Osorio[1]

Title: The mineralizing effect of zinc oxide-modified hydroxyapatite-based sealer on radicular dentin

Affiliations and addresses:

1. Dental School. University of Granada. Colegio Máximo, Campus de Cartuja s/n. 18017 Granada, Spain. Research Institute IBS.

2. University of La Havana, Biomaterials Department, San Lázaro y L. Municipio Plaza de la Revolución La Havana- Cuba.

Corresponding author:

Manuel Toledano-Osorio

Dental School, University of Granada.

Colegio Máximo, Campus de Cartuja s/n 18017 Granada, Spain.

Phone: +34-958243793; Fax: +34-958240908.

E-mail: mtoledano@correo.ugr.es

Abstract

Objective To evaluate the remineralization ability of three endodontic sealer materials at different root dentin regions.

Material and methods Cervical, medial and apical root dentin surfaces were treated with two experimental hydroxyapatite-based cements, containing sodium hydroxide (calcypatite) or zinc oxide (oxipatite); an epoxy resin-based canal sealer, AH Plus; and gutta-percha. Remineralization, at the inner and outer zones of dentin disk surfaces, was studied by nanohardness (*Hi*) and Raman analysis. Nano-roughness and collagen fibrils width measurements were performed. Numerical data, at 24 h or 12 m, were analyzed by ANOVA and Student-Newman-Keuls ($P<0.05$).

Results At the outer and inner zones of cervical dentin treated with oxipatite, the highest *Hi* after 12 m of immersion was achieved. The same group showed the highest intensity of phosphate peak, markers for calcification and crystallinity. Nanoroughness was lower and fibrils diameter was higher at the inner zone of dentin treated with oxipatite. Dentin mineralization occurred in every region of root dentin treated with oxipatite and calcypatite, especially at inner zone of dentin after 12 m.

Conclusions Oxipatite, reinforced the inner root zone at any third of radicular dentin, by increasing both nanohardness and remineralization. When using calcypatite, the highest nanohardness was found at the apical third of the inner root dentin, but the lowest mechanical performance was obtained at the cervical and the medial thirds of the roots. Therefore, application of oxipatite as sealing cement of root canals is recommended.

Clinical relevance Oxipatite, when used as endodontic sealing material, strengthens radicular dentin.

Keywords: Hardness, hydroxyapatite, Raman, remineralization, root dentin, zinc.

Introduction

One of the most important reasons for endodontic failure are cracks and root fracture, leading most often to tooth loss post treatment [1]. Cracks and fractures usually extend from root canal to external root surface throughout the dentin. Cracks are mainly caused by tensile strength [2] due to lateral compaction, stress concentration by surfaces depression and softness of the periodontal ligament, large variations in canal size or shape are found. Studies on single-rooted teeth have shown that a small radius of curvature in the canal may cause early-cracking [3]. Thereby, clinicians have sought to reinforce the remaining tooth structure to increase the fracture resistance of the endodontically treated teeth [4].

Dentin is the major structural component of the tooth. It is composed of hydrated type I organic matrix (18%), an inorganic reinforcing phase of nanocrystalline carbonated apatite (70%), and water (12%). The organic material is 90% collagen [5]. Pivotal features in the hierarchical microstructure of dentin are tubules that radiate outward from the pulp canal to the cementum in the root [6]. Microstructure of dentin is considered as a cylindrical fiber reinforced composite, with the matrix as intertubular dentin and the reinforcements as the tubule lumens and the concomitant peritubular dentin cuff [7]. It is questioned whether loss of structure or changes in dentin properties are responsible for the higher rate of fracture after root canal treatment [8]. With the rigidity of a root weakened by endodontic and restorative instrumentation, the tooth strengthening potential is an important issue [9]. Thereby, one of the main objectives of root canal treatment is to strengthen the cut dentin, to reinforce the dentin structure and to reestablish both mechanical and chemical properties and [10, 11].

New biomaterials for use in endodontics should facilitate dentin remineralization [12, 13] to render better protection to endodontically treated teeth with, most of the time,

a substantial degree of coronal destruction and radicular affectation. The most common used root canal filling material is gutta-percha in combination with a sealer cement [4]. Current root canal sealers, based on epoxy resins such as AH Plus have been recognized as "gold standard" among endodontic materials to obtain adhesion to root dentin surface. Doubts about toxicity and dentin regeneration question their use [14]. Intracanal medicaments containing calcium hydroxide $[Ca(OH)_2]$ are employed in regenerative endodontics [15], trying to penetrate into dentinal tubules, accessory and lateral canals and apical deltas [16], but they seem to produce root fracture. Hydroxyapatite (HAp) based materials have also been considered as potential candidates in the repair and regeneration of hard tissues [17]. Calcium hydroxide powder in association with HAp, as a vehicle, has been proposed for this use. Nevertheless, HAp possesses low mechanical strength and fracture toughness, which is an obstacle for its application in load-bearing areas [17]. Zn-substituted HAp has been shown to possess enhanced bioactivity. This effect makes zinc attractive for use as therapeutic agent in the fields of hard tissue regeneration [18]. Ideally, root canal sealers and root-end filling materials should be bioactive since they are in directly contact with periapical tissues thorough the root apex [19].

The degree and the quality of the mineralization will affect the mechanical properties of dentin. Indeed, the extrafibrilar minerals act as a granular material that can withstand load, but in the absence of intrafibrilar mineralization. Intrafibrilar mineralization is the key factor for ensuring that collagen fibrils have the same mechanical properties as occurs in natural biomineralized dentin [20]. Atomic force microscopy (AFM) assisted nano-indentation does represent a specific applied mean of testing mechanical properties of some materials or substrates [21]. The mechanical properties of root dentin are suspected to vary with location at cervical, middle or apical

third [22]. Functional stresses are predominantly concentrated at the cervical dentin. However, with increasing root dentin removal, the stress patterns shift more apically [23]. Raman spectroscopy is an analytical technique able to measure the molecular composition of dentin containing information regarding chemical changes within the samples [24, 25]. The combination of mechanical and biochemical data with atomic force microscopy (AFM) techniques appears to be a valuable tool to be applied in dentin reinforcement studies [26].

This study is important, as it has been well documented that the composition of dentin is not constant throughout the root, but varies from the cervical to the apical areas, as well as from the inner to the outer dentin [27]. As a result, radicular dentin can perform differently in function of both sealer cement and the selected study region, and differences among root dentin levels should be assessed. The aim of this study was to investigate the nanomechanical, chemical and tribological changes occurring when treating the cervical, medial and apical thirds of radicular dentin after applying two canal sealer cements (calcypatite and oxipatite), one canal sealer (AH Plus) or simply guttacore, used as control without a sealer, at two time points (24 h vs 12 m). The null hypothesis that was established is that no changes in mechanical, chemical and tribological properties were produced at radicular dentin surfaces after the application of the different sealer materials.

Materials and Methods

Specimen preparation and cement application

Forty human mandibular premolars with single roots and vital pulp, extracted for orthodontic or periodontal reasons, without caries lesions were obtained with informed consent from donors (18–25 yr of age), under a protocol approved by the Institution Review Board (#139/CEIH/2016). The teeth were randomly selected and stored at 4ºC in

0.5% chloramine T bacteriostatic/bactericidal solution for up to 1 month. This storage medium was replaced weekly. All teeth were integral and examined using a stereomicroscope (Olympus SZ-CTV, Olympus, Tokyo, Japan) to ascertain the absence of any root fracture or craze lines. The teeth were decoronated using a low-speed diamond saw (Accutom-50 Struers, Copenhagen, Denmark), and the root length was standardized to approximately 12 mm and radiographed at 2 angulations to confirm the presence of a single canals. The root canal treatment began by using Gates Glidden drills (Dentsply Maillefer, Ballaigues, Switzerland), size 2 and 3, in order to shape the coronal third part of the roots. Subsequently, canal patency was achieved using a size 15 Flex-o-file (Dentsply Maillefer, Ballaigues, Switzerland). The working length was measured and established 0.5 mm shorter than apical foramen. The final instrumentation was performed with ProTaper nickel-titanium rotary instruments (Dentsply Maillefer, Ballaigues, Switzerland) up to size F4. At each instrument change, the root canal was irrigated by means of a 27-gauge needle with 0.5 mL of 5% sodium hypochlorite (NaOCl, Panreac, ref. n. 212297), while at the end of canal instrumentation 0.5 mL of a 17% EDTA solution were used for 1 min (MD-Cleanser, Meta Biomed, Chungbuk, Republic of Korea) to remove the smear layer [28]. Each specimen was finally irrigated with 0.5 mL of 5% NaOCl for 1 min, followed with distilled water for one more minute, and dried with paper points (Dentsply Maillefer). The same operator conducted all procedures.

The specimens were divided randomly into 4 groups (n = 10). Two experimental hydroxyapatite-based cements were used: *i*) Calcypatite composed by modified hydroxyapatite particles and a calcium hydroxide-based paste and *ii*) Oxipatite which is a combination of the hydroxyapatite particles and zinc oxide. AH PLUS cement (Dentsply, DeTrey, Konstanz, Germany) was used to conform the third group (*iii*). A control group *(iv)* in which no sealer was applied was also included, in this control group

gutta-percha (GuttaCore) (Dentsply Maillefer, Ballaigues, Switzerland) was compacted into the radicular canal without any sealer or cement. A detailed description of the chemicals and cements is provided in Table 1. Sealers were introduced into the root using a lentulo spiral [29–31], and were compacted into the radicular canal with an endodontic plugger. One size 30 guttacore (GC) cone was placed into the canal to working length, in all groups.

The root surface was entirely covered with nail varnish so that only the apical foramen remained exposed [32]. Each tooth was evaluated radiographically at two angulations to confirm the correct placement of the material along the root canal and the absence of voids. Those teeth that did not meet these requirements were replaced by other root canals properly prepared. Finally, the teeth of each cement subgroup were randomly divided in two groups (n=5) and stored in SBFS solution at 37 °C up to fulfill a period of 24 h or 12 m.

Subvolumes were selected to isolate regions in the cervical root dentin, mid-rot dentin and apical root dentin (12, 9 and 6 mm respectively, above apex), by sectioning perpendicularly to their long axis into 1 mm (±0.1 mm) thick slices.

Nanoindentation

A Hysitron Ti-750D TriboIndenter (Hysitron, Inc., Minneapolis, MN) equipped with a commercial nano-DMA package was employed in this study. The nanoindenter was a Berkovich (three sides pyramidal) diamond tip (tip radius ~20 nm). The nanoindenter tip was calibrated against a fused quartz sample using a quasistatic force setpoint of 5 µN to maintain contact between the tip and the sample surface. On each slab (cervical, middle and apical root dentin), ten indentations were executed in two different mesio-distal positions [20 µm next to radicular cement (outer zone) and 20 µm next to radicular canal (inner zone)] (Figure 1) along the dentin surface in a straight line.

Indentations were performed with a load of 4000 nN and a time function of 10 s. The indenter was progressively (at a constant rate) pressed over the sample up to a peak load of 4000 µN. Specimens were scanned in a hydrated condition. To avoid dehydration a layer of ethylene glycol over the specimen surface was applied, preventing water evaporation during a typical 25-to-30-min scanning period [33]. The distance between each indentation was kept constant by adjusting the distance intervals in 5 (±1) µm steps [34]. Hardness (Hi) data were registered in GPa.

With regard to the nanohardness of the sample, H, it is defined as:

$$H = \frac{F_{max}}{A}$$

where F_{max} is the peak load. In this work, values of nanohardness were automatically calculated by using the software Triboscan Quasi version 8.4.2.0 (Hysitron, Inc). As the normality and homoscedasticity assumptions of the data were valid, numerical data were analyzed with ANOVA and Student-Newman-Keuls multiple comparison tests, with statistical significance preset at $p < 0.05$.

AFM imaging, nanoroughness assessments and fibrils width assessments

Dentin disks were submitted to analysis through an atomic force microscope (AFM Nanoscope V, Digital Instruments, Veeco Metrology group, Santa Barbara, CA, USA) was employed in this study for topography analysis. The imaging process was undertaken inside a wet cell in a fully hydrated state, using the tapping mode, with a calibrated vertical-engaged piezo-scanner (Digital Instrument, Santa Barbara, CA, USA). A 10-nm-radius silicon nitride tip (Veeco) was attached to the end of an oscillating cantilever that came into intermittent contact with the surface at the lowest point of the oscillation. Changes in vertical position of the AFM tip at resonance frequencies near 330 kHz provided the height of the images registered as bright and dark regions. 10 x 10 µm digital images were recorded with a slow scan rate (0.1 Hz). Three digital images (10 µm

× 10 μm) were obtained at randomized areas of the two differentiated sites (inner and outer zone) of each sample disk. For each image, 5 randomized boxes (2 x 2 μm) were created to examine the ID nanoroughness at 24 h and 12 m of storage. Nanoroughness (SRa, in nanometers) was measured with proprietary software (Nanoscope Software, version V7). Collagen fibril diameter was determined from the 10 x 10 μm images by section analysis using data that had been modified only by plane fitting. The collagen fibril diameter was preferentially determined from fibrils that were exposed along their complete widths. Five fibrils were analyzed from each image. Measurements were corrected for tip broadening [35] by the equation e=2r, where e is the error in the horizontal dimension and r is the tip's radius [36]. As the normality and homoscedasticity assumptions of the data were valid, numerical data were analyzed with ANOVA and Student-Newman-Keuls multiple comparison tests, with statistical significance preset at $p < 0.05$.

Raman spectroscopy

The same dentin surfaces were, then, submitted to Raman analysis using a dispersive Raman spectrometer/microscope (Horiba Scientific Xplora, Villeneuve d´Ascq, France). A 785-nm diode laser through a X100/0.90 NA air objective was employed. Raman signal was acquired using a 600-lines/mm grafting centered between 400 and 1700 cm^{-1}. Chemical mapping of the surfaces was performed. For each specimen two different randomized areas 12x12 μm of the sites (inner and outer zone) were mapped using 0.5 μm spacing at X and Y axis (625 points per map). The output from a clustering algorithm was basically a statistical description of the cluster centroids with the number of components in each cluster. The biochemical content of each cluster was analyzed using the average cluster spectra. Chemical mapping was submitted to K-means cluster (KMC) analysis using the multivariate analysis tool (ISys® Horiba), which includes

statistical pattern to derive the independent clusters. The K-means clustering is a method of analysis based on a centroid model which aims to partition "n" observations into "k" clusters in which each observation belongs to the cluster with the nearest mean. The natural groups of components (or data) based on some similarity and the centroids of a group of data sets were found by the clustering algorithm once calculated by the software and the Hierarchical Cluster Analysis (HCA). The observed spectra were described at 400-1700 cm^{-1} with 10 complete overlapping Gaussian lines, suggesting homogeneous data for further calculations [37].

At this point, the mineral component of dentin was assessed after the analysis of the relative presence of mineral, *i.e*, phosphate (960 cm^{-1}) and carbonate (1070 cm^{-1}) peaks and areas, and the relative mineral concentration of phosphate (PO_4^{3-}) referred to phenyl (RMC_p). Additional peaks were measured at 954 cm^{-1}, 956 cm^{-1} and 963 cm^{-1} to analyze the calcification of the extracellular matrix, the additional substituted or amorphous-like apatite species and the stoichiometric hydroxyapatite (HAp), respectively [38–40]. Bands at 430 and 451 cm^{-1} (v_2 mode), and 950 cm^{-1}, representing vibrations of carbonated calcium phosphate and amorphous calcium phosphate in an apatitic lattice, were also assessed [34, 38, 41]. Crystallinity, based on the full width at half maximum (FWHM) of the phosphate band at 960 cm^{-1}, $FWHM_P$ [38] and the gradient in mineral content (GMC) [42] were also assessed. The organic component of dentin was analyzed examining normalization at 1001 cm^{-1}, crosslinking at 1030-1032.7 cm^{-1} (Pyridinium ring vibration). Nature of collagen at the amide III, amide I, and peak at 1340 cm^{-1} indicative of organization, structural differences, altered quality and orientation of α-helices at collagen [43, 44] were also assessed. Complementary indexes concerned collagen at 937 cm^{-1} [39] and t and proteoglycans peaks [38, 39].

Results

Nanoindentation

Nanohardness (*Hi)* of dentin surfaces was influenced by the type of canal filler ($P<0.05$), dentin third ($P<0.05$), dentin zone ($P<0.05$) and by the storage time ($P<0.05$). Interactions between factors were also significant ($P<0.05$). Model reliability was about 65%. Mean and SD of *Hi* at the three different dentin disks (cervical, medial and apical) and zones (inner and outer dentin) are represented in Figure 2.

At the cervical third of radicular dentin, the outer and inner zone of dentin, samples treated with calcypatite attained the highest *Hi* among groups, at 24 h time point. At both the outer and the inner zones of dentin, samples treated with oxipatite achieved the highest *Hi* among groups after 12 m of immersion. At the inner zone of radicular dentin, samples treated with calcypatite decreased *Hi* over time, and those with guttacore and oxipatite increased their *Hi* after 12 m of immersion. At the outer zone of the cervical third, samples treated with oxipatite attained higher *Hi* after 12 m than at 24 h of time point.

At the middle disk of radicular dentin, samples treated with guttacore and calcypatite attained the lowest *Hi* values, at the inner dentin at 12 m time point. Differences were obtained at the outer zone over time, in samples treated with guttacore.

At the apical third of radicular dentin, and after 12 m time point, samples treated with both calcypatite and oxypatite attained the highest *Hi* at the inner zone of dentin. *Hi* increased over time in samples treated with both calcypatite and oxypatite at the outer zone of dentin. At the inner zone of the apical dentin third, only samples treated with calcypatite increased *Hi* from 24 h to 12 m of immersion. After 12 m, samples treated with oxipatite showed similar *Hi* for the middle and apical dentin disks at the inner zone.

Calcypatite attained the highest and the lowest *Hi* values at the apical and medial thirds of radicular dentin, respectively (Fig 2).

AFM imaging, nanoroughness and fibril diameter measurements

Dentin surface roughness (SRa) was influenced by the type of canal filler ($P<0.05$), dentin third ($P<0.05$), dentin zone ($P<0.05$) and by the storage time ($P<0.05$). Interactions between factors were also significant ($P<0.05$). Model reliability for dentin nano- roughness was 0.76. Fibrils width was affected by the type of canal filler ($P<0.01$), dentin third ($P<0.01$), dentin zone ($P<0.01$) and by the storage time ($P<0.05$). Interactions between factors were also significant ($P<0.01$). Model reliability was 0.70.

At 24 h storage time, the highest SRa values at the inner cervical and medial dentin thirds were attained when samples were treated with guttacore (Fig 3). The lowest cervical and apical SRa dentin values corresponded, at the inner zone, with samples treated with both calcypatite and oxipatite. At the inner zone of the apical dentin third, the lowest SRa values were achieved by samples treated with oxipatite, after 12 m (Fig 3). At 24 h of immersion, samples treated with both calcypatite and oxipatite achieved the highest collagen fibril width, at the inner zone, when the cervical and the medial dentin disks were measured (Fig 4). At the apical third, the following trend was achieved: oxipatite > calcypatite > guttacore = AH Plus. However, at 12 m, inner zones of cervical dentin surfaces treated with both calcypatite and oxipatite showed the highest collagen fibril diameter, among groups. Oxipatite promoted the highest collagen fibril diameter at the inner medial and apical dentin thirds. In general, at both inner and outer dentin zones of any dentin third, collagen fibril diameter increased in all groups over time (Fig 4).

AFM images at 10 x 10 µm scan zone revealed strongly mineralized collagen fibrils and total occlusion of dentinal tubules after applying oxipatite (Figs 5a, 5b), regardless the dentin zone. Dentin treated with calcypatite showed mineral deposits

covering the dentin surface at the inner zone, but scarce mineralization at the outer zone of dentin. Median-sized collagen fibrils, especially at middle and apical dentin, were encountered (Figs 5c, 5d). Partially occluded tubules were observed in dentin samples treated with both guttacore and AH Plus (Figs 5e, 5f).

Raman spectroscopy

Samples treated with oxipatite attained higher intensity of phosphate peak, *i.e*, higher mineralization, at the inner dentin zone, regardless of the dentin location, at 12 m of immersion when compared with those obtained at 24 h (Table S1) (Fig 6a). Samples treated with oxipatite obtained the highest intensity of phosphate peak, among groups (Fig 6a), at the inner zone of dentin, and at the outer zone differences were not obtained, at 12 m of storage. HCA Raman images (clusters) (Figs 6c, 6d) and results (centroids) (Figs 6e, 6f) achieved at the inner zone of cervical dentin surface of specimens treated with oxipatite after 12 m of storage showed different variances and higher phosphate peaks, both corresponding to the three distinguishable centroids (HCA_1, HCA_2 and HCA_3), in comparison with the samples treated with calcypatite. After 12 m in samples treated with oxipatite, mineralization attending to the intensity of the phosphate peak at the inner zone of both the apical and medial dentin thirds, was practically similar in all groups, except in the guttacore group which was lower (Table S2). At the outer zone of dentin, samples treated with oxipatite had the highest phosphate peak at the apical third, and those treated with calcypatite at the medial third, among groups (Table S3). Samples treated with oxipatite attained the highest values of markers for calcification (954 cm^{-1}) at any dentin location, at 12 m time point. Similarly, those treated with oxipatite, showed the greatest 963 cm^{-1} peaks (stoichiometric HAP), in general, throughout the whole dentin surface especially at cervical and apical dentin thirds after 12 m of immersion. At cervical dentin, they also obtained the highest crystallinity (lowest FWHM) at any dentin location

(inner or outer), and oxipatite also produced the lowest crystallinity in the medial and apical disks regardless of the dentin location. Crystallinity increased at both inner cervical and apical dentin thirds over time.

After 12 m of immersion, amorphous calcium phosphate (950 cm^{-1} and 956) was higher at the inner zone of both cervical and medial dentin thirds than at the apical third when samples were treated with oxipatite. After using calcypatite, 950 cm^{-1} band was higher at the inner zone of the apical dentin that at cervical and medial thirds, and at the outer zone was similar to samples when oxipatite was used. Those specimens treated with oxipatite attained the highest vibrations of carbonated calcium phosphate (451 cm^{-1}) throughout the whole inner wall of radicular dentin (cervical, medial and apical thirds). Calcypatite promoted the highest 451 cm^{-1} bands at the outer dentin at both cervical and apical dentin. Oxipatite promoted the highest intensity of phosphate (Figs 7a, S1a, S1b), carbonate peaks and carbonate substitution for phosphate (GMC) after 12 m of storage, at any dentin location. In general, samples treated with calcypatite and AH Plus achieved higher relative mineral concentration (RMCp) values than the rest of the groups after 12 m of storage, at both apical and cervical dentin locations (Figs 7b, S1c) (Table S4).

After 12 m of immersion, samples treated with oxipatite attained the highest vibrations of the organic content (575 cm^{-1}) throughout the whole inner and outer walls of radicular dentin (cervical, medial and apical thirds), and the highest crosslinking, *i.e*, peak values (1030-1032.7 cm^{-1}) (Figs 7c, S1e, S1f). Treatment with calcypatite promoted a decrease of 575 cm^{-1} band in dentin, except at the apical inner dentin, over time. On the contrary, this band (575 cm^{-1}), increased over time when oxipatite was used and assessed at any inner dentin third. The highest presence of collagen (937 cm^{-1}) and its most favorable molecular orientation throughout the dentin wall was also obtained after treating with oxipatite at any type of dentin location. The highest maturity (amide I) (AI)

and organization of collagen (AI/AIII), at the apical third of dentin (regardless the dentin zone) was achieved when samples were treated with oxipatite. Similarly, the greatest intensity peak corresponding to the presence of proteoglycans (1062 cm^{-1}) was obtained after treating with oxipatite at any type of dentin location, after 12 m of immersion (Figs 7d, S1g, S1h).

Discussion

Two experimental HAp-based cements, (*i*) calcypatite (composed by modified HAp particles and a calcium hydroxide-based paste), (*ii*) oxipatite (a combination of the HAp particles, and zinc oxide), and *(iii)* an epoxy resin-based canal sealer, AH Plus sealer were compared in this study.

The intrinsic material properties of root dentin do have spatial variations, being altered by ageing. Dentin undergoes gradual spatial transition in its material properties. In the root, a decreasing trend in mineral content from the cervical dentin to the apical dentin has been found. Hence, the mechanical properties of root dentin are suspected to vary with location [22] and it was confirmed by our results. The cervical third of root dentin is a potential failure site due to deformation, strain and stress concentration [45]. The general high *Hi* at the cervical third of dentin, and at the inner zone of apical dentin after using oxipatite, in comparison with the rest of the materials, at 12 m of immersion (Fig 2) may be correlated, in the present research, with a remineralizing effect [46]. This effect was linked to mineral precipitation (Ca, P and Zn) within the demineralized organic matrix (Fig 5a). It has been previously stated that nanohardness recovery at the dentin substrate is only produced if functional remineralization occurred [20, 47]. This mineralization increase coincided after 12 m storage time with *i),* the highest collagen fibril width at the inner zone within any dentin third, after 12 m of immersion (Figs 4,

16

5a). The growing of fibrils width and dentin remineralization are commonly associated [48, 49]; *ii),* the lowest dentin nanoroughness, which decreased at the apical third of dentin when oxipatite was applied, but without significant difference (Fig 3); *iii),* the highest intensity of both phosphate peak (Figs 6a, 7a, S1a, S1b) (Table S1) at the inner zone of root dentin, thus denoting greater presence of this mineral; and with *iv),* the highest peaks in dentin treated with oxipatite, at both v_l 954 and 963 cm^{-1} Raman intensities. These values became associated to the greatest calcification of the dentin matrix (peak at 954 cm^{-1}) [39], at the expense of both stoichiometric hydroxyapatite (HAp) (963 cm^{-1}) [40] and additional substituted or amorphous-like apatite species (peak at 956 cm^{-1}) [40] (Table S1) (Fig 6e). This remineralization event is a dynamic process in which amorphous phase formation, phase stabilization, and transition of calcium phosphate continuously occur [50]. Amorphous Ca/P provides a local ion-rich environment which is considered favorable for *in situ* generation of prenucleation clusters, succeeding further dentin remineralization [51]. Generally, the HAp with poor crystallinity has the best bioactivity, biocomopatibility and biodegradability if compared with the stoichiometric HAp. This finding concurred with a decrease of FWHM$_p$, *i.e.,* higher crystallinity at cervical dentin (Table S1), and was linked to an improvement of mechanical properties [52, 53], as it did occur in the present research (Fig 2). On the other hand, the increase in fibril diameter, detected in the control group, is associated to an increase of mineralization [54] and to a decrease of dentin nanoroughness. Components of guttacore include zinc oxide, among others (>50 wt%, information from manufacturers). Zinc oxide has been demonstrated to be bioactive, promoting functional biomineralization of hard tissues and hence, increasing mechanical properties as nanohardness and Young's modulus [20, 47]. As a result, advanced functional

mineralization is linked to intrafibrillar mineralization, higher collagen fibrils width and lower roughness values.

Oxipatite also promoted the most prominent carbonate band around 1070 cm^{-1} and carbonate substitution for phosphate (GMC) at any kind of dentin, after 12 m time point (Table S1). Carbonated apatite is a precursor of HAp, but when it is precipitated in the presence of zinc an exchange between Zn^{2+} and Ca^{2+} occurs *in vitro* forming a substituted apatite compound [55]. It is speculated that zinc may have acted as crystal growth inhibitor facilitating amorphous calcium phosphate stabilization, intrafibrillar mineralization of collagen. These data correlate with an augmentation of bands at 451 cm^{-1} (v_2 mode), assigned to vibration of carbonate calcium phosphate in apatite lattice [40] (Table S1), which provides both bioactivity, intrafibrilar mineralization and HAp stabilization [53].

The maximal tensile strength tend to develop in the apical region of the root [2]. The strains at the apical part of the root were 2.5- and 6-fold higher than the strains at middle-root and cervical parts, respectively [2]. Instrumenting the apical third reduced the fracture strength of the root [4]. Apical third of root dentin samples treated with calcypatite achieved, after 12 m of storage, the highest *Hi* at the inner region (Fig 2), just where calcypatite promoted the greatest bands corresponding to both the phosphate peak (960cm^{-1}) and to the amorphous calcium phosphate (950 cm^{-1}) (Table S3). This inner canal wall concentrates the stress distribution to occur in the canal root [2]. Calcium hydroxide, present in calcypatite, induces matrix formation and mineralization through the release of bone morphogenetic proteins, cytokines, and some specific tissue grown factors [56]. Calcypatite behaves as a hydrophilic material [10] able to set in a moist environment (dentinal fluid); wetness is essential to induce bioactivity and apatite precipitation [57]. Moreover, the setting reaction of calcypatite involves the continuous

formation of hydration products that contribute to reducing the micro-channels in the cement bulk [58]. The hydration products may, *i)* react with dentinal ions (Ca and P) and reduce marginal gaps, improving the seal of the apical third by calcium phosphate precipitates [59] (Fig 6c) or by means of formed zinc-based salts [53]; and *ii),* provide the mechanical interlock of the dentin interface and the obliteration of dentinal tubules in the absence of smear layer, previously removed by EDTA irrigation. As in the present study, leakage of fluids through lateral radicular walls was restricted by varnish placement during the experimental procedure, this particular result should be interpreted with caution and deserves additional research. The hydroxyl group is considered the most important component of $Ca(OH)_2$ as it provides an alkaline environment, which encourages repair and active calcification [60]. The hydroxyls ions are able to diffuse throughout the whole root dentin and toward the surface of the root [16]. We speculate that calcypatite in case of immature apexes or apical lesions can perform as self-repairing dental cement, able to promote deposition of calcium phosphate at the dentin substrate (Figs 5c, 5d). This approach provides a promising preventive contribution in regenerative endodontics [13], as this modified HAp calcium hydroxide-based cement promoted both hardness and bioactivity. On the other hand, apical dentin treated with AH Plus attained the lowest *Hi* and, thereby, the lowest functional remineralization [47]. Similarly, root dentin treated with AH Plus (Fig 5f) did not exhibit higher fracture resistance than samples which were un-instrumented and unfilled [61]. The lack of any bioactivity potential is probably because mostly calcium present in this material are not in the ionized form [19, 62]. Nevertheless, oxipatite promoted the highest maturity (AI) and organization of collagen (AI/AIII) at the apical third of dentin (Table S1).

Results from Raman evaluation confirmed that the relative mineral concentration (RMC) attained at both inner and outer region of any dentin third (Fig 7b) was higher

after treating dentin surfaces with both calcypatite (Table S3) or AH Plus (Table S4) than with oxipatite. These changes in the chemical composition cause an increase in apparent brittleness of the tissue and reduction in damage tolerance and lowest resistance to fracture [63]. Thus, any fracture or strong discontinuity in the mechanical properties at the microscopic level of the restoration, restorative interface of dental substrate would definitely have consequences in the overall function that takes place at the macroscopic level. Similarly, oxipatite also promoted the highest vibration of organic content (575 cm^{-1}) [64], collagen crosslinking (1032 cm^{-1}) [65] (Figs 7c, S1e, S1f), molecular orientation (1340 cm^{-1}) [44] and proteoglycans (1062 cm^{-1}) [39] (Figs 7d, S1g, S1h) at any kind of root dentin third, after 12 m time point. High levels of collagen cross-linking could be the cause of improved mechanical properties of dentin [66]. Moreover, Zn has demonstrated to inhibit matrix-metalloproteases and to increase the crosslinking of the collagen [44]. Proteoglycans act as bonding agents between the collagen network and the HAp crystals [67] (Table S1). All these results imply that even when oxipatite attained the highest presence of phosphate, the RMCp was not the highest, as oxiapatite also exerted increases and changes in concentration and quality of collagen. Highest RMCp in the chemical composition cause an increase in apparent brittleness of the tissue and reduction in damage tolerance and lowest resistance to fracture, as it occurs when calcypatite is applied. At the medial disk of radicular dentin, samples treated with guttacore (Fig 5e) and calcypatite attained the lowest *Hi* values (Fig 2) and scarce remineralization (Tables S2, S3), at the inner dentin after 12 m time point, meanwhile *Hi* differences were not obtained at the outer zone over time (Fig 2). Guttapercha has been found to present little or no capacity to reinforce roots after treatment [4].

Biomechanical and biochemical integrity at instrumented and filled root dentin has not been adequately assessed. To our knowledge, no previous studies have evaluated

nanohardness and biochemical changes combined with morphological and tribological nano-characterization with different endodontic cements at different levels of root dentin. The null hypothesis must be rejected. Relative to complementary experimental techniques that ultimately illustrate the clinical reaction of radicular dentin, Field-emission SEM (FESEM), dark-field TEM (DF-TEM), High Resolution TEM (HRTEM), Scanning Transmission Electron Microscopy (STEM) and micro-XRD (μ-XRD), and fuzzy c-means cluster analysis (FCA) should be incorporated into our methodology, for future strategies of research. Therefore, the lack of these techniques may be considered as a limitation of the present study.

Conclusion

Within the limitations of the present study, it can be concluded that obturating instrumented root canals with oxipatite, a combination of hydroxyapatite particles and zinc oxide, reinforces the inner root zone at any third of radicular dentin, by increasing both nanohardness and remineralization. Calcypatite showed the highest nanohardness at the apical third of the inner root dentin, but the lowest mechanical performance obtained in the cervical and the medial thirds of the radicular dentin. Therefore, oxipatite is preferable as obturating cement of root canals.

Compliance with ethical standards

Ethical approval: All procedures performed in the present study, involving human participants, were in accordance with the ethical standards of the institutional and/or national research committee and with the 1964 Helsinki declaration and its later amendments or comparable ethical standards. This article does not contain any studies with animals performed by any of the authors.

Informed consent: Informed consent was obtained from all individual participants included in the study.

References

1. Huynh N, Li F-C, Friedman S, Kishen A (2018) Biomechanical Effects of Bonding Pericervical Dentin in Maxillary Premolars. J Endod 44:659–664. https://doi.org/10.1016/j.joen.2018.01.002

2. Brosh T, Metzger Z, Pilo R (2018) Circumferential root strains generated during lateral compaction with stainless steel vs. nickel-titanium finger spreaders. Eur J Oral Sci 126:518–525. https://doi.org/10.1111/eos.12569

3. Chai H, Tamse A (2018) Vertical Root Fracture in Buccal Roots of Bifurcated Maxillary Premolars from Condensation of Gutta-percha. J Endod 44:1159–1163. https://doi.org/10.1016/j.joen.2018.03.017

4. Patil P, Banga KS, Pawar AM, et al (2017) Influence of root canal obturation using gutta-percha with three different sealers on root reinforcement of endodontically treated teeth. An in vitro comparative study of mandibular incisors. J Conserv Dent JCD 20:241–244. https://doi.org/10.4103/JCD.JCD_233_16

5. Marshall GW, Marshall SJ, Kinney JH, Balooch M (1997) The dentin substrate: structure and properties related to bonding. J Dent 25:441–458

6. Kinney JH, Nalla RK, Pople JA, et al (2005) Age-related transparent root dentin: mineral concentration, crystallite size, and mechanical properties. Biomaterials 26:3363–3376. https://doi.org/10.1016/j.biomaterials.2004.09.004

7. Nalla RK, Kinney JH, Ritchie RO (2003) Effect of orientation on the in vitro fracture toughness of dentin: the role of toughening mechanisms. Biomaterials 24:3955–3968

8. Cheron RA, Marshall SJ, Goodis HE, Peters OA (2011) Nanomechanical properties of endodontically treated teeth. J Endod 37:1562–1565. https://doi.org/10.1016/j.joen.2011.08.006

9. Chu C-Y, Kuo T-C, Chang S-F, et al (2010) Comparison of the microstructure of crown and root dentin by a scanning electron microscopic study. J Dent Sci 5:14–20. https://doi.org/10.1016/S1991-7902(10)60003-7

10. Toledano M, Pérez-Álvarez MC, Aguilera FS, et al (2017) A zinc oxide-modified hydroxyapatite-based cement facilitated new crystalline-stoichiometric and amorphous apatite precipitation on dentine. Int Endod J 50 Suppl 2:e109–e119. https://doi.org/10.1111/iej.12807

11. Toledano M, Osorio R, Pérez-Álvarez M-C, et al (2018) A zinc-doped endodontic cement facilitates functional mineralization and stress dissipation at the dentin surface. Med Oral Patol Oral Cirugia Bucal 23:e646–e655. https://doi.org/10.4317/medoral.22751

12. Gandolfi MG, Ciapetti G, Taddei P, et al (2010) Apatite formation on bioactive calcium-silicate cements for dentistry affects surface topography and human marrow stromal cells proliferation. Dent Mater Off Publ Acad Dent Mater 26:974–992. https://doi.org/10.1016/j.dental.2010.06.002

13. Osorio R, Sauro S, Watson TF, Toledano M (2016) Polyaspartic acid enhances dentine remineralization bonded with a zinc-doped Portland-based resin cement. Int Endod J 49:874–883. https://doi.org/10.1111/iej.12518

14. Hakki SS, Bozkurt BS, Ozcopur B, et al (2013) The response of cementoblasts to calcium phosphate resin-based and calcium silicate-based commercial sealers. Int Endod J 46:242–252. https://doi.org/10.1111/j.1365-2591.2012.02122.x

15. Kitikuson P, Srisuwan T (2016) Attachment Ability of Human Apical Papilla Cells to Root Dentin Surfaces Treated with Either 3Mix or Calcium Hydroxide. J Endod 42:89–94. https://doi.org/10.1016/j.joen.2015.08.021

16. Miñana M, Carnes DL, Walker WA (2001) PH changes at the surface of root dentin after intracanal dressing with calcium oxide and calcium hydroxide. J Endod 27:43–45. https://doi.org/10.1097/00004770-200101000-00015

17. Al-Sanabani JS, Madfa AA, Al-Sanabani FA (2013) Application of calcium phosphate materials in dentistry. Int J Biomater 2013:876132. https://doi.org/10.1155/2013/876132

18. Matsunaga K (2008) First-principles study of substitutional magnesium and zinc in hydroxyapatite and octacalcium phosphate. J Chem Phys 128:245101. https://doi.org/10.1063/1.2940337

19. Viapiana R, Guerreiro-Tanomaru JM, Hungaro-Duarte MA, et al (2014) Chemical characterization and bioactivity of epoxy resin and Portland cement-based sealers with niobium and zirconium oxide radiopacifiers. Dent Mater Off Publ Acad Dent Mater 30:1005–1020. https://doi.org/10.1016/j.dental.2014.05.007

20. Balooch M, Habelitz S, Kinney JH, et al (2008) Mechanical properties of mineralized collagen fibrils as influenced by demineralization. J Struct Biol 162:404–410. https://doi.org/10.1016/j.jsb.2008.02.010

21. Poon B, Rittel D, Ravichandran G (2008) An analysis of nanoindentation in linearly elastic solids. Int J Solids Struct 45:6018–6033. https://doi.org/10.1016/j.ijsolstr.2008.07.021

22. Xu H, Zheng Q, Shao Y, et al (2014) The effects of ageing on the biomechanical properties of root dentine and fracture. J Dent 42:305–311. https://doi.org/10.1016/j.jdent.2013.11.025

23. Ossareh A, Rosentritt M, Kishen A (2018) Biomechanical studies on the effect of iatrogenic dentin removal on vertical root fractures. J Conserv Dent JCD 21:290–296. https://doi.org/10.4103/JCD.JCD_126_18

24. Kunstar A, Leijten J, van Leuveren S, et al (2012) Recognizing different tissues in human fetal femur cartilage by label-free Raman microspectroscopy. J Biomed Opt 17:116012. https://doi.org/10.1117/1.JBO.17.11.116012

25. Toledano M, Aguilera FS, Osorio E, et al (2015) On modeling and nanoanalysis of caries-affected dentin surfaces restored with Zn-containing amalgam and in vitro oral function. Biointerphases 10:041004. https://doi.org/10.1116/1.4933243

26. Wang L, Zhao Y, Mei L, et al (2017) Effect of application time of maleic acid on smear layer removal and mechanical properties of root canal dentin. Acta Odontol Scand 75:59–66. https://doi.org/10.1080/00016357.2016.1248789

27. Verdelis K, Eliades G, Oviir T, Margelos J (1999) Effect of chelating agents on the molecular composition and extent of decalcification at cervical, middle and apical root dentin locations. Endod Dent Traumatol 15:164–170

28. O'Connell MS, Morgan LA, Beeler WJ, Baumgartner JC (2000) A comparative study of smear layer removal using different salts of EDTA. J Endod 26:739–743. https://doi.org/10.1097/00004770-200012000-00019

29. Mestres G, Aguilera FS, Manzanares N, et al (2014) Magnesium phosphate cements for endodontic applications with improved long-term sealing ability. Int Endod J 47:127–139. https://doi.org/10.1111/iej.12123

30. Monticelli F, Osorio R, Toledano M, et al (2010) Sealing properties of one-step root-filling fibre post-obturators vs. two-step delayed fibre post-placement. J Dent 38:547–552. https://doi.org/10.1016/j.jdent.2010.03.014

31. Vizgirda PJ, Liewehr FR, Patton WR, et al (2004) A comparison of laterally condensed gutta-percha, thermoplasticized gutta-percha, and mineral trioxide aggregate as root canal filling materials. J Endod 30:103–106. https://doi.org/10.1097/00004770-200402000-00010

32. Bouillaguet S, Shaw L, Barthelemy J, et al (2008) Long-term sealing ability of Pulp Canal Sealer, AH-Plus, GuttaFlow and Epiphany. Int Endod J 41:219–226. https://doi.org/10.1111/j.1365-2591.2007.01343.x

33. Ryou H, Niu L-N, Dai L, et al (2011) Effect of biomimetic remineralization on the dynamic nanomechanical properties of dentin hybrid layers. J Dent Res 90:1122–1128. https://doi.org/10.1177/0022034511414059

34. Toledano M, Sauro S, Cabello I, et al (2013) A Zn-doped etch-and-rinse adhesive may improve the mechanical properties and the integrity at the bonded-dentin interface. Dent Mater Off Publ Acad Dent Mater 29:e142-152. https://doi.org/10.1016/j.dental.2013.04.024

35. Habelitz S, Balooch M, Marshall SJ, et al (2002) In situ atomic force microscopy of partially demineralized human dentin collagen fibrils. J Struct Biol 138:227–236

36. Takeyasu K, Omote H, Nettikadan S, et al (1996) Molecular imaging of Escherichia coli F0F1-ATPase in reconstituted membranes using atomic force microscopy. FEBS Lett 392:110–113

37. Ager JW, Nalla RK, Breeden KL, Ritchie RO (2005) Deep-ultraviolet Raman spectroscopy study of the effect of aging on human cortical bone. J Biomed Opt 10:034012. https://doi.org/10.1117/1.1924668

38. Toledano M, Osorio R, Osorio E, et al (2016) Advanced zinc-doped adhesives for high performance at the resin-carious dentin interface. J Mech Behav Biomed Mater 62:247–267. https://doi.org/10.1016/j.jmbbm.2016.05.013

39. Kunstar A, Leijten J, van Leuveren S, et al (2012) Recognizing different tissues in human fetal femur cartilage by label-free Raman microspectroscopy. J Biomed Opt 17:116012. https://doi.org/10.1117/1.JBO.17.11.116012

40. Timlin JA, Carden A, Morris MD, et al (2000) Raman Spectroscopic Imaging Markers for Fatigue-Related Microdamage in Bovine Bone. Anal Chem 72:2229–2236. https://doi.org/10.1021/ac9913560

41. Lussi A, Schlueter N, Rakhmatullina E, Ganss C (2011) Dental erosion--an overview with emphasis on chemical and histopathological aspects. Caries Res 45 Suppl 1:2–12. https://doi.org/10.1159/000325915

42. Schwartz AG, Pasteris JD, Genin GM, et al (2012) Mineral distributions at the developing tendon enthesis. PloS One 7:e48630. https://doi.org/10.1371/journal.pone.0048630

43. Salehi H, Terrer E, Panayotov I, et al (2013) Functional mapping of human sound and carious enamel and dentin with Raman spectroscopy. J Biophotonics 6:765–774. https://doi.org/10.1002/jbio.201200095

44. Wang C, Wang Y, Huffman NT, et al (2009) Confocal Laser Raman Microspectroscopy of Biomineralization Foci in UMR 106 Osteoblastic Cultures Reveals Temporally Synchronized Protein Changes Preceding and Accompanying Mineral Crystal Deposition. J Biol Chem 284:7100–7113. https://doi.org/10.1074/jbc.M805898200

45. Kaushik M, Kumar U, Sharma R, et al (2018) Stress distribution in endodontically treated abfracted mandibular premolar restored with different cements and crowns: A three-dimensional finite element analysis. J Conserv Dent JCD 21:557–561. https://doi.org/10.4103/JCD.JCD_206_18

46. Toledano M, Osorio R, Osorio E, et al (2017) Ions-modified nanoparticles affect functional remineralization and energy dissipation through the resin-dentin interface. J Mech Behav Biomed Mater 68:62–79. https://doi.org/10.1016/j.jmbbm.2017.01.026

47.   Bertassoni LE, Stankoska K, Swain MV (2012) Insights into the structure and composition of the peritubular dentin organic matrix and the lamina limitans. Micron Oxf Engl 1993 43:229–236. https://doi.org/10.1016/j.micron.2011.08.003

48.   Clarkson BH, McCurdy SP, Gaz D, Hand AR (1993) Effects of phosphoprotein on collagen fibril formation in vitro. Arch Oral Biol 38:737–743. https://doi.org/10.1016/0003-9969(93)90068-W

49.   He G, George A (2004) Dentin Matrix Protein 1 Immobilized on Type I Collagen Fibrils Facilitates Apatite Deposition in Vitro. J Biol Chem 279:11649–11656. https://doi.org/10.1074/jbc.M309296200

50.   Tramini P, Pélissier B, Valcarcel J, et al (2000) A Raman spectroscopic investigation of dentin and enamel structures modified by lactic acid. Caries Res 34:233–240. https://doi.org/10.1159/000016596

51.   Liu Y, Tjäderhane L, Breschi L, et al (2011) Limitations in bonding to dentin and experimental strategies to prevent bond degradation. J Dent Res 90:953–968. https://doi.org/10.1177/0022034510391799

52.   Low I-M (2004) Depth-Profiling of Crystal Structure, Texture, and Microhardness in a Functionally Graded Tooth Enamel. J Am Ceram Soc 87:2125–2131. https://doi.org/10.1111/j.1151-2916.2004.tb06369.x

53.   Toledano M, Aguilera FS, Osorio E, et al (2015) Self-etching zinc-doped adhesives improve the potential of caries-affected dentin to be functionally remineralized. Biointerphases 10:031002. https://doi.org/10.1116/1.4926442

54.   Bertassoni LE, Habelitz S, Pugach M, et al (2010) Evaluation of surface structural and mechanical changes following remineralization of dentin. Scanning 32:312–319. https://doi.org/10.1002/sca.20199

55. Mayer I, Apfelbaum F, Featherstone JDB (1994) Zinc ions in synthetic carbonated hydroxyapatites. Arch Oral Biol 39:87–90. https://doi.org/10.1016/0003-9969(94)90040-X

56. Li Y, Chen X, Fok A, et al (2015) Biomimetic Mineralization of Recombinamer-Based Hydrogels toward Controlled Morphologies and High Mineral Density. ACS Appl Mater Interfaces 7:25784–25792. https://doi.org/10.1021/acsami.5b07628

57. Tay FR, Pashley DH, Rueggeberg FA, et al (2007) Calcium phosphate phase transformation produced by the interaction of the portland cement component of white mineral trioxide aggregate with a phosphate-containing fluid. J Endod 33:1347–1351. https://doi.org/10.1016/j.joen.2007.07.008

58. Gandolfi MG, Prati C (2010) MTA and F-doped MTA cements used as sealers with warm gutta-percha. Long-term study of sealing ability. Int Endod J 43:889–901. https://doi.org/10.1111/j.1365-2591.2010.01763.x

59. Tay FR, Pashley DH (2007) Monoblocks in root canals: a hypothetical or a tangible goal. J Endod 33:391–398. https://doi.org/10.1016/j.joen.2006.10.009

60. Mohammadi Z, Dummer PMH (2011) Properties and applications of calcium hydroxide in endodontics and dental traumatology. Int Endod J 44:697–730. https://doi.org/10.1111/j.1365-2591.2011.01886.x

61. Jainaen A, Palamara JEA, Messer HH (2009) The effect of resin-based sealers on fracture properties of dentine. Int Endod J 42:136–143. https://doi.org/10.1111/j.1365-2591.2008.01496.x

62. Gandolfi MG, Taddei P, Modena E, et al (2013) Biointeractivity-related versus chemi/physisorption-related apatite precursor-forming ability of current root end filling materials. J Biomed Mater Res B Appl Biomater 101:1107–1123. https://doi.org/10.1002/jbm.b.32920

63. Ryou H, Amin N, Ross A, et al (2011) Contributions of microstructure and chemical composition to the mechanical properties of dentin. J Mater Sci Mater Med 22:1127–1135. https://doi.org/10.1007/s10856-011-4293-8

64. Ramakrishnaiah R, Rehman G ur, Basavarajappa S, et al (2015) Applications of Raman Spectroscopy in Dentistry: Analysis of Tooth Structure. Appl Spectrosc Rev 50:332–350. https://doi.org/10.1080/05704928.2014.986734

65. Daood U, Iqbal K, Nitisusanta LI, Fawzy AS (2013) Effect of chitosan/riboflavin modification on resin/dentin interface: spectroscopic and microscopic investigations. J Biomed Mater Res A 101:1846–1856. https://doi.org/10.1002/jbm.a.34482

66. Toledano M, Cabello I, Osorio E, et al (2018) Zn-containing polymer nanogels promote cervical dentin remineralization

67. Bakland LK, Andreasen JO (2012) Will mineral trioxide aggregate replace calcium hydroxide in treating pulpal and periodontal healing complications subsequent to dental trauma? A review. Dent Traumatol Off Publ Int Assoc Dent Traumatol 28:25–32. https://doi.org/10.1111/j.1600-9657.2011.01049.x

Figure captions

Fig. 1 Schematic representation of specimen preparation. Tooth coronal section was discarded. Three disks of cervical, medial and apical dentin were obtained. Inner and outer dentin zones were assessed

Fig. 2 Nanohardness (*Hi*) at the different experimental root dentin-treated surfaces. Identical lower case indicates no significant differences among different materials at the same dentin third (cervical, medial and apical) and zones (inner and outer) after 24 hours. Identical capital letter indicates no significant differences between different materials at the same dentin third (cervical, medial and apical) and zones (inner and outer) after 6 months. Identical number indicates no significant differences between different zones (inner *vs* outer) with the same materials at the same storage time. Asterisks indicate significant differences between the different storage periods (24 h *vs* 12 m) with the same material at the same zone (inner or outer). Identical symbols indicate no significant differences between the different dentin thirds (cervical, medial and apical) at the same zone (inner and outer) and period (24 h and 12 m) within the same material, after Student-Newman-Keuls or Student t tests respectively (p<0.05).

Fig. 3 Nanoroughness at the different experimental root dentin-treated surfaces. Identical lower case indicates no significant differences among different materials at the same dentin third (cervical, medial and apical) and zones (inner and outer) after 24 hours. Identical capital letter indicates no significant differences between different materials at the same dentin third (cervical, medial and apical) and zones (inner and outer) after 6 months. Identical number indicates no significant differences between different zones (inner *vs* outer) with the same materials at the same storage time. Asterisks indicate

significant differences between the different storage periods (24 h *vs* 12 m) with the same material at the same zone (inner or outer). Identical symbols indicate no significant differences between the different dentin thirds (cervical, medial and apical) at the same zone (inner and outer) and period (24 h and 12 m) within the same material, after Student-Newman-Keuls or Student t tests respectively (p<0.05).

Fig. 4 Fibrils diameter at the different experimental root dentin-treated surfaces. Identical lower case indicates no significant differences among different materials at the same dentin third (cervical, medial and apical) and zones (inner and outer) after 24 hours. Identical capital letter indicates no significant differences between different materials at the same dentin third (cervical, medial and apical) and zones (inner and outer) after 6 months. Identical number indicates no significant differences between different zones (inner *vs* outer) with the same materials at the same storage time. Asterisks indicate significant differences between the different storage periods (24 h *vs* 12 m) with the same material at the same zone (inner or outer). Identical symbols indicate no significant differences between the different dentin thirds (cervical, medial and apical) at the same zone (inner and outer) and period (24 h and 12 m) within the same material, after Student-Newman-Keuls or Student t tests respectively (p<0.05).

Fig. 5 10 x 10 μm top-view and surface plot image of cervical dentin, inner (**a**) and outer (**b**) zones, obtained by AFM after applying oxipatite, at 12 m time point. Peritubular (PD) and intertubular (ID) dentin mineralization is evidenced. Intratubular dentin (TD) is totally occluding the dentinal tubules (asterisks). Collagen fibrils, the bandwidth of the collagen fibrils and the wider bandwidth (faced arrows) with the staggered pattern of collagen fibrils are shown (pointer). Tubules density was lower in the outer zone. 10 x 10

µm top-view and surface plot image of apical dentin, inner (**c**) and outer (**d**) zones, obtained by AFM after applying calcypatite, at 12 m time point. Extended mineral depleted areas (asterisks) are reflected. Mineral tubular occlusion (pointers) may be observed at the dentin surface. Tubules figured completely occluded. Wider bandwidth of the collagen fibrils and the staggered pattern of collagen fibrils are shown (faced arrows). Scarce number of opened dentinal tubules were observed at the outer zone of dentin. Peritubular (PD) and intertubular (ID) dentin appeared well differentiated. Strong peritubular ring was formed at the entrance of tubules (arrows). 10 x 10 µm top-view and surface plot image of medial dentin obtained by AFM after applying only guttacore (**e**) or AH Plus canal sealer (**f**), at 12 m time point. Some dentinal tubules appeared partially filled (single arrows) or totally empty (pointers). Peritubular rings were evident (double arrows). Collagen fibrils (faced arrows) were observed crossing the intertubular dentin (ID)

Fig. 6 2D micro-Raman map of the phosphate peak (961 cm^{-1}) intensities at the groups of samples treated with oxipatite (**a**) and calcypatite (**b**) of the inner zone at the cervical third of radicular dentin, after 12 m of storage. Color mapping from hierarchical cluster analysis (HCA) images corresponding to dentin surfaces treated with oxipatite (**c**) and calcypatite (**d**), both in conditions similar to those reflected in (a) and (b). Three levels of HCA clustering are shown. Areas of distinct colors have differences in Raman spectral distribution and chemical composition. Each cluster, corresponding to a different dentin remineralization stage, is assigned to a different color (red, green, and blue), thus obtaining a false color-image of the substrate on the basis of similar spectral features. Spectra from hierarchical cluster analysis (HCA) results of dentin surfaces treated with oxipatite (**e**) and calcypatite (**f**) both in conditions similar to those reflected in (a) and (b)

Fig. 7 Raman intensitites of phosphate peak (961cm^{-1}) (**a**), phosphate relative mineral concentration (RMC) (**b**), pyridinium (**c**) and proteoglycans (**d**) at cervical (a,c), middle (d) and apical (b) thirds of radicular dentin at inner and outer zones of dentin, after 24 h and 12 m time periods. The peaks values were normalized to the intensity of the Amide II band near 1510 cm^{-1}

Table 1. Materials and chemicals used in this study.

Product details			
Calcypatite	Calcium hydroxide (CaOH)₂	**Basic formulation per 100 gr**	
		Content and quantity (g)	*Percentage (%)*
		Calcium hydroxide 45.0 g Carbowax 400 40.0 g Titanium dioxide 7.0 g Aerosil 1.0 g Barium Sulphate 7.0 g	42.5
	Hydroxyapatite modified particles	*Component and percentage*	
		Calcium 39.2 % Phosphorus 18.3 % Magnesium < 0.1 % Sodium < 0.1 % Silicon 0.001-0.03 % Other minor components < 0.005 % Molar relation Ca/P 1.66	57.5
Oxiapatite	Zinc oxide (ZnO)	**Basic formulation per 100 gr**	
		Content and quantity (g)	*Percentage (%)*
		Zinc oxide (ZnO) 39.61 g Titanium dioxide 5.8 g Carbowax 400 40.0 g Aerosil 2.0 g Barium sulphate 14.8 g	42.5
	Hydroxyapatite modified particles	*Component and percentage*	
		Calcium 39.2 % Phosphorus 18.3 % Magnesium < 0.1 % Sodium < 0.1 % Silicon 0.001-0.03 % Other minor components < 0.005 % Molar relation Ca/P 1.66	57.5
AH Plus (Dentsply, DeTrey, Konstanz, Germany)		Paste A: diepoxide, calcium tungstate, zirconium oxide, aerosil, pigment (Fe oxide) Paste B: 1-adamantane amine, N,N'-dibenzyl-5-oxa-nonandiamine-1,9, TCD-Diamine, calcium tungstate, zirconium oxide, aerosil, silicone oil	
NaOCl 5% (Panreac Química SA, Barcelona, Spain)			
EDTA 17% (Sigma Aldrich, St. Louis, MO, USA)			
Simulated Body Fluid Solution (SBFS) pH=7.45	Sigma Aldrich, St. Louis, MO, USA	NaCl 8.035 g NaHCO₃ 0.355 g K₂HPO₄·3H₂O 0.231 g, MgCl₂·6H₂O 0.311 g 1.0 M – HCl 39 ml Tris 6.118 g	
	Panreac Química SA, Barcelona, Spain	KCl 0.225 g CaCl₂ 0.292 g Na₂SO₄ 0.072 g 1.0 M – HCl 0–5 ml	

Abbreviations: SBFS: simulated body fluid solution; TCD: 3(4),8(9)-bis(aminomethyl)triciclo[5.2.1.02,6] Decane; NaCl: sodium chloride; NaHCO₃: sodium bicarbonate; KCl: potassium chloride; K₂HPO₄·3H₂O: potassium phosphate dibasic trihydrate; MgCl₂·6H₂O: magnesium chloride hexahydrate; HCl: hydrogen chloride; CaCl₂: Calcium chloride; Na₂SO₄: sodium sulfate; Tris: tris(hydroxylmethyl) aminomethane

Figure 1

1. Cervical disk

2. Medial disk

3. Apical disk

Cement

Dentin

Radicular canal

Endodontic cement
and/or GuttaCore

Outer zone for analysis
(20 μm from
cement junction)

Inner zone for analysis
(20 μm from cement junction)
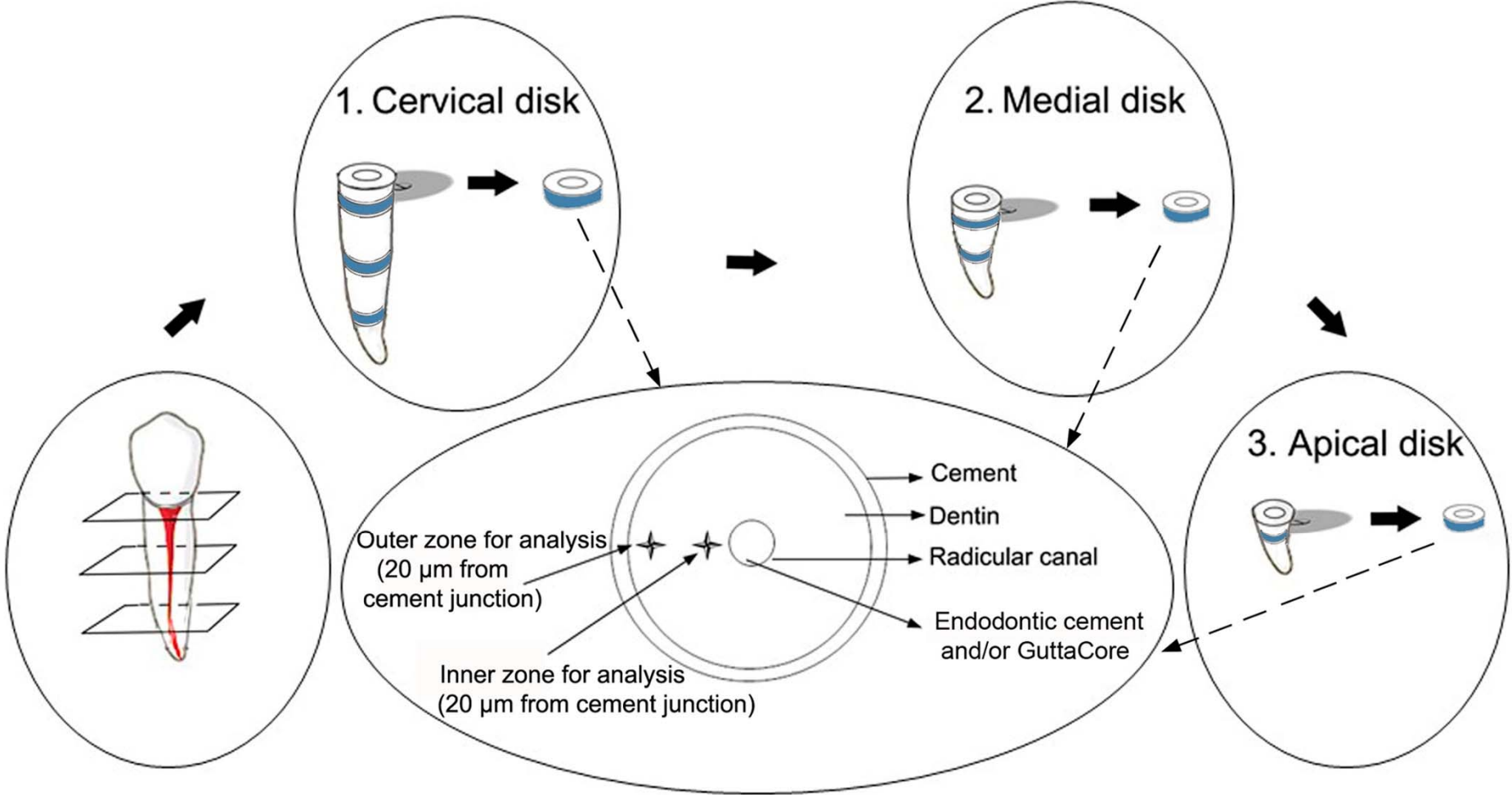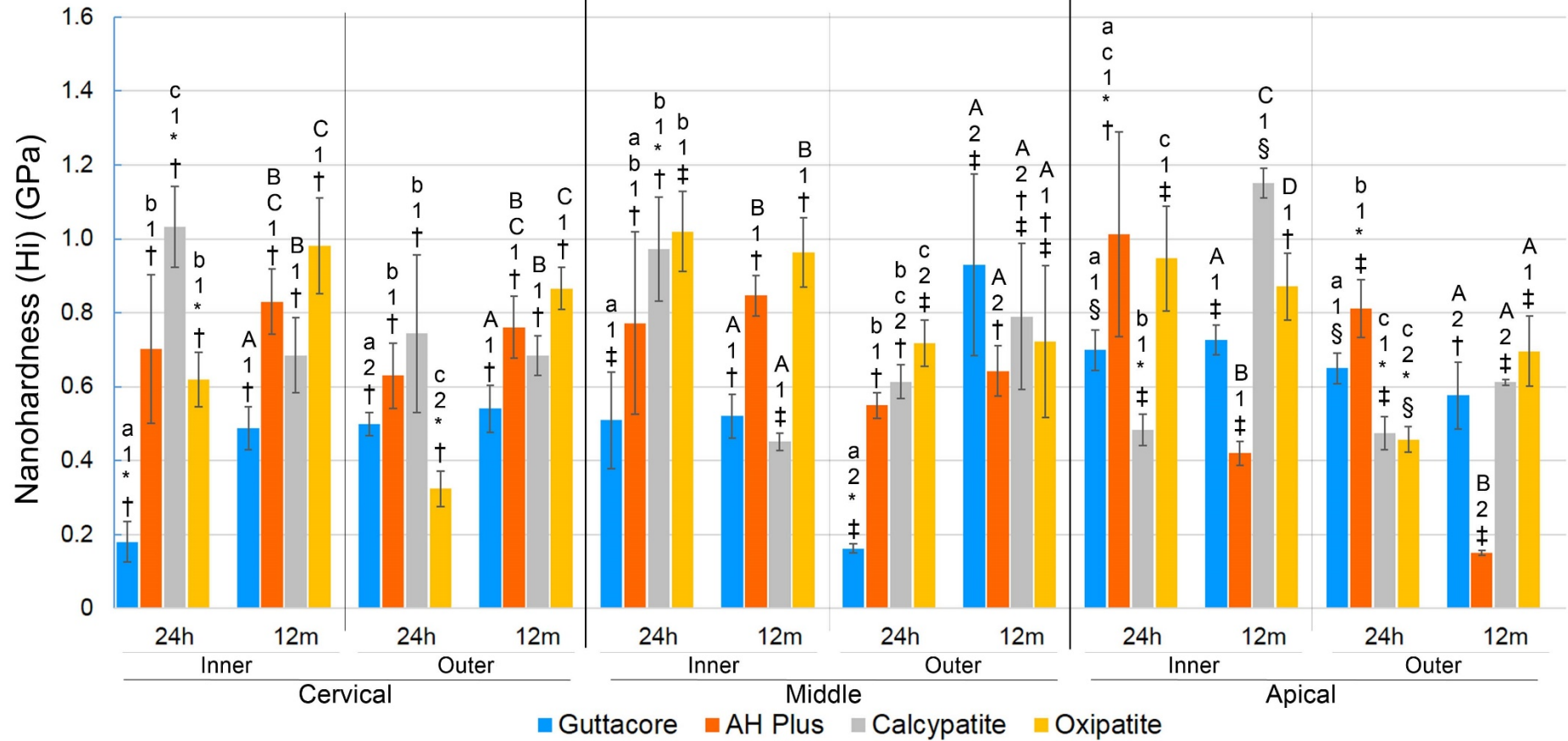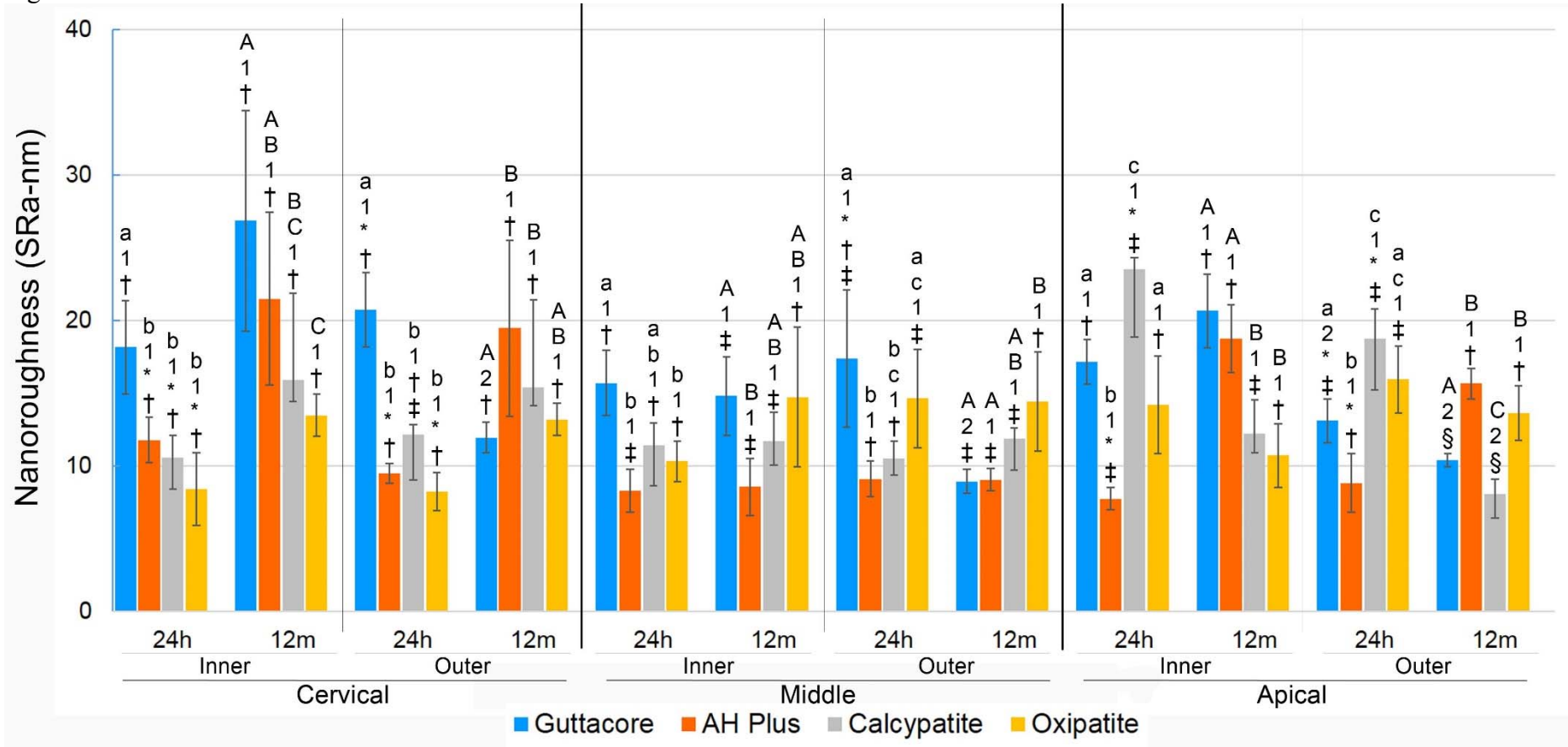
Figure 2

Figure 3

Figure 4
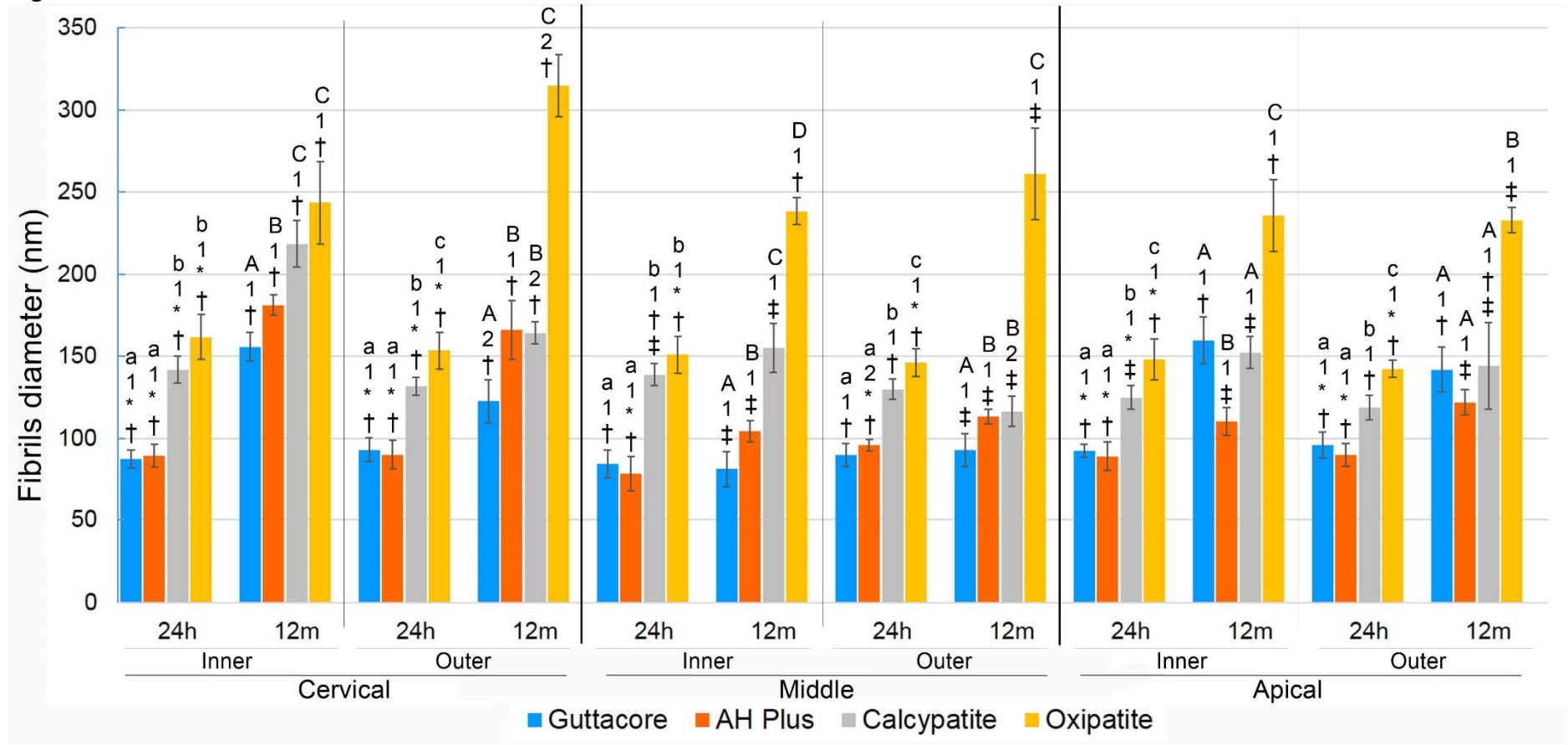
Figure 5
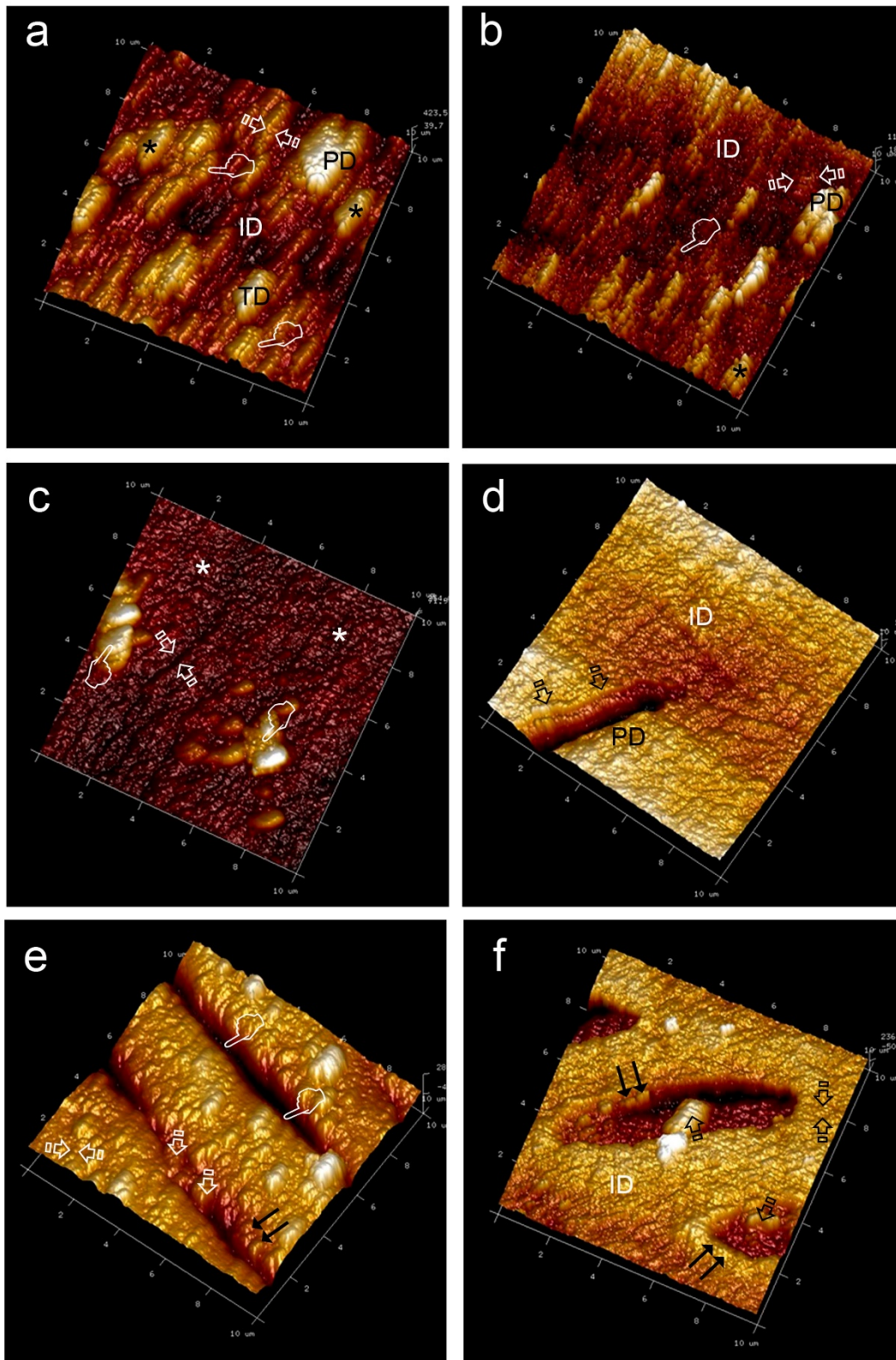
Figure 6
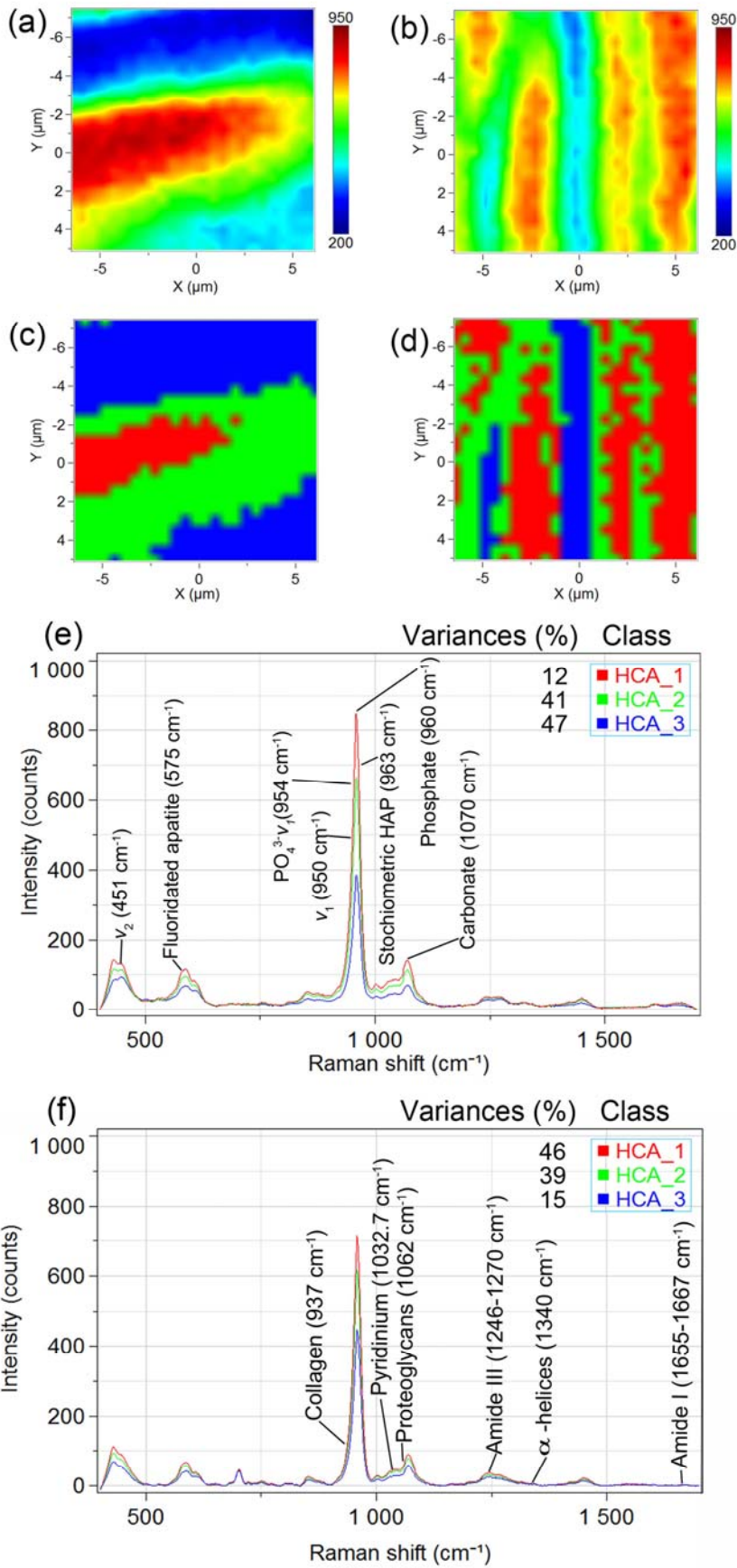
Figure 7
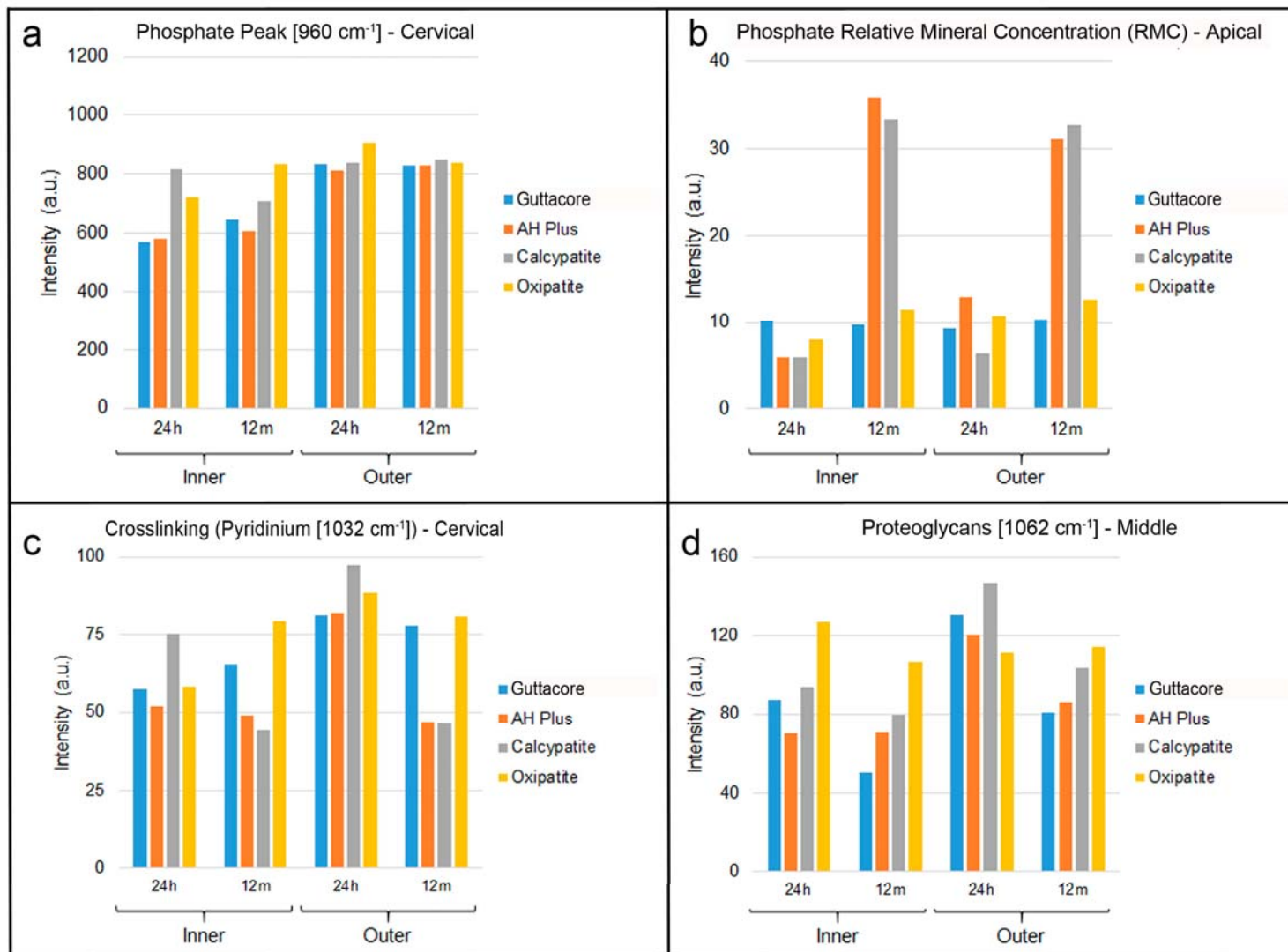
Figure S1: Raman intensitites of phosphate peak (961cm^{-1}) at middle dentin (**a**), phosphate peak (961cm^{-1}) at apical dentin (**b**), phosphate relative mineral concentration at cervical dentin (RMC) (**c**), phosphate relative mineral concentration at middle dentin (RMC) (**d**), pyridinium at middle dentin (**e**), pyridinium at apical dentin (**f**), proteoglycans at cervical dentin (**g**), and proteoglycans at apical dentin (**h**). The peaks values were normalized to the intensity of the Amide II band near 1510 cm^{-1}.
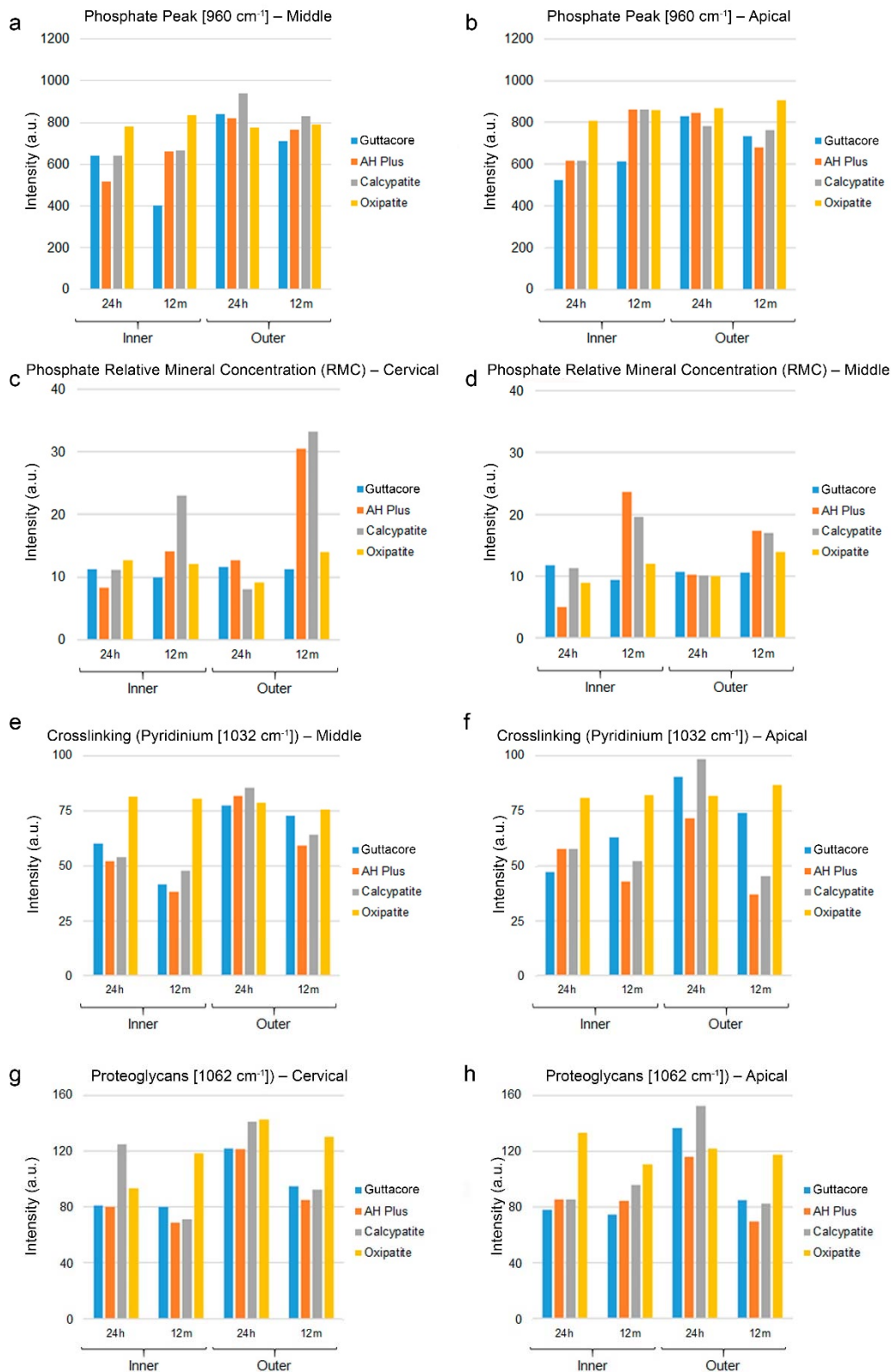
Table S1. Raman intensities (in arbitrary units) of mineral and organic components in different disks from radicular dentin treated with oxipatite after 24 h and 12 m of storage.

| MINERAL COMPONENTS | | | Cervical | | | | Middle | | | | Apical | | | |
| | | | Inner | | Outer | | Inner | | Outer | | Inner | | Outer | |
			24h	12m	24h	12m	24h	12m	24h	12m	24h	12m	24h	12m
Relative Presence of Mineral	Phosphate [960 cm⁻¹]	Peak	720.66	834.17	909.83	839.64	779.76	835.21	777.62	789.28	807.68	858.84	867.78	905.71
		Area	19428.90	20316.40	21178.80	19251.00	22542.90	24689.70	22731.90	21278.70	23181.20	21785.20	22082.00	26773.80
		RMC_P	12.68	12.07	9.16	13.99	8.93	12.04	10.05	13.88	8.00	11.44	10.80	12.55
	Carbonate [1070 cm⁻¹]	Peak	111.49	138.01	164.03	141.29	143.11	137.04	128.60	142.54	152.523	138.79	145.87	154.50
		Area	4689.00	5447.64	8491.73	5441.60	7457.62	5696.29	6124.97	5412.49	8276.42	6195.93	5976.09	5909.48
Phosphate Crystallinity ($FWHM_P$)			20.59	18.59	19.45	17.49	22.09	22.59	22.33	20.59	21.93	19.36	19.42	22.59
GMC (Ratio 1070/960)			0.15	0.17	0.18	0.17	0.18	0.16	0.17	0.18	0.19	0.16	0.17	0.17
$v2$[451 cm⁻¹]			74.35	129.32	91.65	80.36	87.59	122.00	85.44	109.40	93.50	112.48	82.64	87.00
Fluoridated Apatite [575 cm⁻¹]			73.11	103.84	97.15	95.08	85.92	91.43	88.71	66.88	74.16	105.09	93.78	93.02
$v1$[950 cm⁻¹]			433.14	561.86	514.34	625.06	506.05	448.79	485.63	449.60	506.15	441.17	480.79	457.22
$v1$[954 cm⁻¹]			638.19	723.78	791.32	797.76	718.95	683.93	642.92	691.44	724.36	698.50	747.57	720.80
$v1$[956 cm⁻¹]			691.30	788.12	863.78	849.93	763.15	757.34	712.66	751.41	780.31	778.48	820.14	808.28
$v1$[963 cm⁻¹]			633.19	670.04	798.20	589.11	652.39	783.30	649.38	704.15	704.76	794.46	766.56	856.21
$v1$[1003 cm⁻¹]			55.75	68.27	99.09	58.71	88.32	69.68	78.41	56.86	97.97	74.06	80.22	74.08
[1104 cm⁻¹]			24.43	29.61	58.26	33.41	49.73	32.02	43.78	34.01	54.40	41.69	43.20	42.95

| ORGANIC COMPONENTS | | Cervical | | | | Middle | | | | Apical | | | |
| | | Inner | | Outer | | Inner | | Outer | | Inner | | Outer | |
		24h	12m	24h	12m	24h	12m	24h	12m	24h	12m	24h	12m
Normalization	Phenyl [1001 cm⁻¹]	56.85	69.10	99.36	60.01	87.31	69.34	77.41	56.86	101.02	75.05	80.35	72.16
Crosslinking	Pyridinium [1032 cm⁻¹]	58.00	79.27	88.06	80.74	81.29	80.57	78.70	75.51	80.66	81.97	81.67	86.63
Nature of collagen	A-III [1246-1270 cm⁻¹]	39.10	34.20	60.54	54.65	45.23	35.88	41.92	52.22	41.83	46.99	51.46	48.25
	A-I [1655-1667 cm⁻¹]	16.34	16.95	82.23	30.02	32.90	16.49	29.41	28.07	44.84	30.43	30.39	28.95
	Ratio AI/AIII	0.42	0.50	1.36	0.55	0.73	0.46	0.70	0.54	1.07	0.65	0.59	0.60
	α-helices [1340 cm⁻¹]	16.75	13.75	22.12	16.20	12.52	14.82	12.62	13.66	16.45	11.83	16.16	13.43
Complementary indexes	Collagen [937 cm⁻¹]	143.97	176.16	206.16	180.66	183.66	169.19	165.42	151.40	193.98	163.05	189.19	173.49
	Proteoglycans [1062 cm⁻¹]	93.71	118.59	142.92	130.25	127.03	105.89	110.65	113.80	133.13	110.44	122.16	117.76

Abbreviations: RMC: Relative Mineral Concentration between mineral/Phenyl (1003 cm⁻¹); $FWHM_P$: Full-width half-maximum of the phosphate band at 960 cm⁻¹; GMC: Gradient in mineral content; A: amide; AGEs: advanced glycation end products. The peaks values had been normalized to the intensity of the Amide II band near 1510 cm⁻¹.

Table S2. Raman intensities (in arbitrary units) of mineral and organic components in different disks from radicular dentin treated with guttacore after 24 h and 12 m of storage.

			Cervical				Middle				Apical			
			Inner		Outer		Inner		Outer		Inner		Outer	
			24h	12m	24h	12m	24h	12m	24h	12m	24h	12m	24h	12m
MINERAL COMPONENTS	**Relative Presence of Mineral**	Phosphate [960 cm^{-1}] / Peak	567.90	644.16	833.64	828.20	641.00	400.76	838.55	709.46	523.07	614.48	830.03	734.24
		Area	14247.90	16304.70	21080.40	20409.40	15707.20	10143.70	24067.20	17706.40	13539.10	15553.40	21325.30	18173.20
		RMC$_P$	11.23	10.03	11.59	11.30	11.81	9.43	10.69	10.54	10.21	9.70	9.33	10.27
		Carbonate [1070 cm^{-1}] / Peak	92.77	92.45	140.52	109.27	100.88	55.75	154.33	89.88	88.72	84.80	152.74	97.00
		Area	4514.41	4494.96	5546.62	4421.74	4857.99	2710.65	6490.89	4224.88	3864.22	4122.94	6979.44	4465.21
	Phosphate Crystallinity (FWHM$_P$)		19.15	19.32	19.30	18.81	18.70	19.32	21.93	19.05	19.76	19.32	19.61	18.89
	GMC (Ratio 1070/960)		0.16	0.14	0.17	0.13	0.16	0.14	0.18	0.13	0.17	0.14	0.18	0.13
	v2[451 cm^{-1}]		60.25	77.87	80.26	112.66	69.75	57.86	134.33	63.66	76.71	70.08	121.96	63.55
	Fluoridated Apatite [575 cm^{-1}]		59.18	83.10	89.11	66.29	66.62	52.67	70.10	78.73	43.79	76.82	70.55	74.95
	v1[950 cm^{-1}]		399.55	430.74	517.50	437.81	432.36	275.11	496.95	398.74	368.69	395.35	546.25	404.72
	v1[954 cm^{-1}]		503.53	552.02	689.69	625.30	600.61	348.55	750.73	556.74	462.29	515.78	712.51	565.65
	v1[956 cm^{-1}]		543.38	603.34	764.16	718.27	632.17	378.81	809.66	632.68	498.47	567.97	779.87	644.29
	v1[963 cm^{-1}]		453.63	528.89	687.51	702.28	526.85	323.90	723.87	580.50	427.46	510.72	668.75	622.08
	v1[1003 cm^{-1}]		48.97	61.67	70.62	69.04	52.27	40.14	76.22	65.27	51.25	60.51	86.98	70.22
	[1104 cm^{-1}]		24.92	30.42	40.24	36.89	24.65	19.34	45.13	33.53	24.28	30.34	52.23	34.47

			Cervical				Middle				Apical			
			Inner		Outer		Inner		Outer		Inner		Outer	
			24h	12m	24h	12m	24h	12m	24h	12m	24h	12m	24h	12m
ORGANIC COMPONENTS	**Normalization**	Phenyl [1001 cm^{-1}]	50.59	64.20	71.94	73.27	54.26	42.49	78.45	67.33	51.21	63.35	89.01	71.49
	Crosslinking	Pyridinium [1032 cm^{-1}]	57.40	65.37	81.08	77.70	60.10	41.53	77.27	72.69	47.16	63.02	90.49	74.04
	Nature of collagen	A-III [1246-1270 cm^{-1}]	33.24	40.81	51.21	59.20	38.01	30.20	58.38	51.51	34.67	43.54	50.53	47.97
		A-I [1655-1667 cm^{-1}]	18.87	22.29	32.03	32.83	18.47	16.21	36.65	29.53	16.61	23.53	32.72	25.96
		Ratio AI/AIII	0.57	0.55	0.63	0.55	0.49	0.54	0.63	0.57	0.48	0.54	0.65	0.54
		α-helices [1340 cm^{-1}]	10.45	12.15	15.21	17.11	11.27	9.86	10.31	15.19	8.96	13.70	6.32	14.58
	Complementary indexes	Collagen [937 cm^{-1}]	133.45	146.58	166.54	144.90	144.80	97.77	176.55	128.37	133.14	136.99	187.08	133.95
		Proteoglycans [1062 cm^{-1}]	81.24	80.34	122.12	95.10	87.33	50.37	130.13	80.77	78.00	74.55	136.71	85.20

Abbreviations: RMC: Relative Mineral Concentration between mineral/Phenyl (1003 cm^{-1}); FWHM$_P$: Full-width half-maximum of the phosphate band at 960 cm^{-1}; GMC: Gradient in mineral content; A: amide; AGEs: advanced glycation end products. The peaks values had been normalized to the intensity of the Amide II band near 1510 cm^{-1}.

Table S3. Raman intensities (in arbitrary units) of mineral and organic components in different disks from radicular dentin treated with calcypatite after 24 h and 12 m of storage.

| | | | Cervical | | | | Middle | | | | Apical | | | |
| | | | Inner | | Outer | | Inner | | Outer | | Inner | | Outer | |
			24h	12m	24h	12m	24h	12m	24h	12m	24h	12m	24h	12m
MINERAL COMPONENTS	**Relative Presence of Mineral**	Phosphate [960 cm^{-1}] — Peak	816.18	707.16	836.00	849.29	640.23	666.35	941.56	830.33	615.93	862.17	781.29	763.19
		Phosphate [960 cm^{-1}] — Area	21097.80	20347.20	21371.80	22226.60	16643.90	17439.00	24070.30	21730.40	15745.80	22016.80	19973.00	19252.00
		Phosphate [960 cm^{-1}] — RMC$_P$	11.20	23.05	8.04	33.28	11.27	19.55	10.13	17.01	5.91	33.20	6.40	32.67
		Carbonate [1070 cm^{-1}] — Peak	141.79	89.66	158.04	114.19	109.08	91.32	167.16	120.38	99.11	115.22	167.54	101.41
		Carbonate [1070 cm^{-1}] — Area	6937.08	3630.09	7088.91	4154.71	5616.97	4087.29	7589.14	4561.82	4445.71	3894.57	11747.80	3843.18
	Phosphate Crystallinity (FWHM$_P$)		19.73	21.98	19.52	19.98	19.85	19.98	19.52	19.98	19.52	19.49	19.52	19.26
	GMC (Ratio 1070/960)		0.17	0.13	0.19	0.13	0.17	0.14	0.18	0.14	0.16	0.13	0.21	0.13
	$v2$[451 cm^{-1}]		82.25	86.84	77.50	126.07	68.81	80.36	92.82	98.37	74.50	107.22	85.38	101.05
	Fluoridated Apatite [575 cm^{-1}]		83.33	58.30	79.01	65.02	70.18	59.53	96.22	75.51	73.12	81.11	78.71	72.87
	$v1$[950 cm^{-1}]		554.13	499.10	545.75	526.42	437.74	431.48	582.52	535.57	424.97	527.74	512.55	453.96
	$v1$[954 cm^{-1}]		703.74	636.77	704.90	716.09	556.58	560.70	774.68	716.18	542.55	718.32	661.47	626.06
	$v1$[956 cm^{-1}]		766.12	685.61	774.72	793.24	605.17	619.03	861.97	785.42	588.42	798.60	726.25	699.47
	$v1$[963 cm^{-1}]		663.62	601.99	685.36	664.11	510.88	535.71	765.04	645.43	484.62	679.58	644.48	607.93
	$v1$[1003 cm^{-1}]		72.26	29.31	101.71	24.96	55.14	30.90	91.05	46.84	90.32	24.44	118.46	21.58
	[1104 cm^{-1}]		37.02	16.16	46.96	25.70	27.01	17.94	54.79	34.41	30.80	23.63	71.05	24.45

| | | | Cervical | | | | Middle | | | | Apical | | | |
| | | | Inner | | Outer | | Inner | | Outer | | Inner | | Outer | |
			24h	12m	24h	12m	24h	12m	24h	12m	24h	12m	24h	12m
ORGANIC COMPONENTS	**Normalization**	Phenyl [1001 cm^{-1}]	72.86	30.67	104.04	25.52	56.81	34.09	92.05	48.81	104.14	25.97	122.09	23.36
	Crosslinking	Pyridinium [1032 cm^{-1}]	75.37	43.93	97.25	46.24	54.00	47.70	85.30	64.19	57.72	52.06	98.41	45.24
	Nature of collagen	A-III [1246-1270 cm^{-1}]	33.86	38.68	48.81	63.31	33.27	34.83	58.57	57.88	35.46	57.95	54.59	64.29
		A-I [1655-1667 cm^{-1}]	17.00	3.92	27.13	12.33	16.80	5.24	43.37	18.33	15.89	9.55	34.60	11.76
		Ratio AI/AIII	0.50	0.10	0.56	0.19	0.50	0.15	0.74	0.32	0.45	0.16	0.63	0.18
		α-helices [1340 cm^{-1}]	14.68	7.19	20.30	10.59	15.53	6.12	21.98	9.41	7.57	8.51	16.97	10.42
	Complementary indexes	Collagen [937 cm^{-1}]	189.47	118.75	205.72	124.65	148.87	124.85	195.29	147.62	137.68	129.67	217.77	112.26
		Proteoglycans [1062 cm^{-1}]	124.92	71.51	141.37	92.47	93.72	79.48	146.42	102.90	85.50	95.76	152.75	82.50

Abbreviations: RMC: Relative Mineral Concentration between mineral/Phenyl (1003 cm^{-1}); FWHM$_P$: Full-width half-maximum of the phosphate band at 960 cm^{-1}; GMC: Gradient in mineral content; A: amide; AGEs: advanced glycation end products. The peaks values had been normalized to the intensity of the Amide II band near 1510 cm^{-1}.

Table S4. Raman intensities (in arbitrary units) of mineral and organic components in different disks of radicular dentin treated with AH Plus after 24 h and 12 m of storage.

MINERAL COMPONENTS				Cervical				Middle				Apical			
				Inner		Outer		Inner		Outer		Inner		Outer	
				24h	12m	24h	12m	24h	12m	24h	12m	24h	12m	24h	12m
Relative Presence of Mineral	Phosphate [960 cm⁻¹]	Peak		579.02	605.23	810.17	829.46	516.73	659.06	820.79	765.10	615.93	860.95	844.86	679.77
		Area		17084.30	15142.60	20270.00	21683.70	13079.20	17229.20	24217.80	20001.10	15745.80	21540.60	21365.30	17538.70
		RMC_P		8.31	14.11	12.70	30.47	5.06	23.63	10.21	17.32	5.91	35.80	12.86	31.05
	Carbonate [1070 cm⁻¹]	Peak		93.28	81.39	143.51	114.10	82.78	93.56	141.66	112.61	99.11	105.93	137.54	92.89
		Area		4535.14	3276.81	5778.00	3831.26	3687.55	3434.12	6310.57	4245.36	4445.71	3397.43	5634.27	3051.49
Phosphate Crystallinity ($FWHM_P$)				22.54	19.10	19.10	19.96	19.32	19.96	22.54	19.96	19.52	19.10	19.30	19.70
GMC (Ratio 1070/960)				0.16	0.13	0.18	0.14	0.16	0.14	0.17	0.15	0.16	0.12	0.16	0.14
$v2$[451 cm⁻¹]				65.16	72.27	69.85	120.12	50.48	107.54	121.23	81.82	74.50	147.49	79.97	90.14
Fluoridated Apatite [575 cm⁻¹]				51.98	42.40	82.64	68.28	51.81	51.24	62.72	77.24	73.12	71.04	84.89	61.58
$v1$[950 cm⁻¹]				377.12	369.83	504.74	518.10	335.05	444.20	513.30	476.03	424.97	469.80	505.40	412.19
$v1$[954 cm⁻¹]				485.03	495.05	670.44	705.12	434.54	580.35	675.63	650.40	542.55	673.02	683.51	569.38
$v1$[956 cm⁻¹]				532.16	551.20	743.26	779.12	477.86	631.58	747.40	717.76	588.42	765.33	764.20	633.90
$v1$[963 cm⁻¹]				488.80	504.55	662.39	638.25	425.98	513.16	695.91	586.97	484.62	708.06	704.50	520.98
$v1$[1003 cm⁻¹]				67.50	41.63	61.99	25.20	90.22	27.00	77.02	40.74	90.32	20.17	64.57	18.30
[1104 cm⁻¹]				26.52	20.58	35.10	25.91	28.66	17.27	39.94	26.70	30.80	21.39	35.61	19.06

ORGANIC COMPONENTS			Cervical				Middle				Apical			
			Inner		Outer		Inner		Outer		Inner		Outer	
			24h	12m	24h	12m	24h	12m	24h	12m	24h	12m	24h	12m
Normalization	Phenyl [1001 cm⁻¹]		69.65	42.88	63.81	27.23	102.13	27.89	80.43	44.17	104.14	24.05	65.70	21.89
Crosslinking	Pyridinium [1032 cm⁻¹]		51.94	48.91	81.92	46.85	52.06	38.12	81.84	59.21	57.72	42.95	71.50	36.92
Nature of collagen	A-III [1246-1270 cm⁻¹]		33.22	33.91	49.85	61.03	37.59	44.84	48.85	47.75	35.46	63.62	47.37	61.26
	A-I [1655-1667 cm⁻¹]		14.82	6.08	29.63	10.53	16.32	5.39	30.74	13.10	15.88	12.63	27.82	10.79
	Ratio AI/AIII		0.45	0.18	0.59	0.17	0.43	0.12	0.63	0.27	0.45	0.20	0.59	0.18
	α-helices [1340 cm⁻¹]		9.23	5.13	11.64	9.25	12.21	7.20	8.77	6.10	7.57	11.67	21.28	12.24
Complementary indexes	Collagen [937 cm⁻¹]		127.55	111.48	166.38	122.05	113.89	117.80	173.80	117.86	137.68	101.84	159.37	97.94
	Proteoglycans [1062 cm⁻¹]		80.07	69.03	121.39	85.00	70.12	70.37	120.48	85.78	85.50	84.62	115.95	69.62

Abbreviations: RMC: Relative Mineral Concentration between mineral/Phenyl (1003 cm⁻¹); $FWHM_P$: Full-width half-maximum of the phosphate band at 960 cm⁻¹; GMC: Gradient in mineral content; A: amide; AGEs: advanced glycation end products. The peaks values had been normalized to the intensity of the Amide II band near 1510 cm⁻¹.